frontiers in Marine Science

ORIGINAL RESEARCH
published: 29 May 2018
doi: 10.3389/fmars.2018.00179

Temporal Variability in Net Primary Production in an Upwelling Area off Central Chile (36°S)

Giovanni Testa[1,2,3], *Italo Masotti*[3,4] *and Laura Farías*[2,3]*

[1] Graduate Program in Oceanography, Department of Oceanography, University of Concepción, Concepción, Chile, [2] Department of Oceanography, Faculty of Natural and Oceanographic Sciences, University of Concepción, Concepción, Chile, [3] Center for Climate and Resilience Research, University of Chile, Santiago de Chile, Chile, [4] Facultad de Ciencias del Mar y de Recursos Naturales, Universidad de Valparaíso, Viña del Mar, Chile

The temporal variability of Net Primary Production (NPP) off central Chile (36°S, 73°W), an area subjected to seasonal coastal upwelling, was analyzed using monthly *in situ* ^{13}C incubations within the photic zone, along with bio-oceanographic variables from a fixed time series station; and satellite NPP estimations (NPPE) from the Vertically Generalized Production Model between 2006 and 2015. NPP and NPPE rates varied from 0.03 to 18.29 and from 0.45 to 9.07 g C m^{-2} d^{-1}, respectively. Both rates were fairly well correlated with each other ($r^2 = 0.61$), but when these data were separated into two periods, higher r^2 value was found during winter ($r^2 = 0.70$) with respect to the rest of the year ($r^2 = 0.24$); the latter correlation was partially due to increased weekly NPPE variability during active and relaxed upwelling events. NPP rates along with other biophysical variables allowed for a division of the annual cycle into three distinct periods: September to January (high productivity, mean integrated NPP rates of 4.0 g C m^{-2} d^{-1}), February to March (intermediate productivity, mean integrated NPP rates of 1.4 g C m^{-2} d^{-1}), and May to August (basal level, mean integrated NPP rates of 0.5 g C m^{-2} d^{-1}). NPP appeared to be partially controlled by nutrient inputs, either from upwelling (September-April) and river discharge (May-August), maintaining high NPP rates throughout the entire year, with an annual mean NPP rate of 1.1 kg C m^{-2} yr^{-1}. In this region, El Niño Southern Oscillation events did not appear to impact the NPP interannual variability.

Keywords: primary production rates, coastal upwelling, river discharge, El Niño Southern oscillation, central Chile

OPEN ACCESS

Edited by:
Alejandro A. Murillo, EMBL Heidelberg, Germany

Reviewed by:
X. Antón Álvarez-Salgado, Consejo Superior de Investigaciones Científicas (CSIC), Spain
Laura Lorenzoni, University of South Florida, United States

***Correspondence:**
Laura Farías
laura.farias@udec.cl

Specialty section:
This article was submitted to Coastal Ocean Processes, a section of the journal Frontiers in Marine Science

Received: *07 February 2018*
Accepted: *07 May 2018*
Published: *29 May 2018*

Citation:
Testa G, Masotti I and Farías L (2018) Temporal Variability in Net Primary Production in an Upwelling Area off Central Chile (36°S). Front. Mar. Sci. 5:179. doi: 10.3389/fmars.2018.00179

INTRODUCTION

The Eastern Boundary Upwelling Systems (EBUS) are considered the most productive regions in the world's oceans and sustain the greatest portion of global fishery production (Pauly and Christensen, 1995; Cubillos et al., 1998b). This high productivity is mainly the result of the coastal upwelling process by which subsurface, nutrient-rich waters ascend to the surface in response to wind stress on surface water, fertilizing waters in the photic zone and promoting phytoplankton blooms. Lachkar and Gruber (2012) identified equatorward alongshore wind, eddy activity, the width of the continental shelf and mixed layer depth as key physical and environmental factors controlling Net Primary Production (NPP) in the EBUS. On the other hand, Messié and Chavez (2015) detected wind-driven macronutrient supply, iron provision,

temperature, light and offshore export as main drivers of time-space NPP variability in the EBUS.

The coastal upwelling systems off Chile extend over a wide latitudinal range (∼19–40°S), along irregular coastline with diverse topographic features (including canyons and the continental shelf) and variable river runoff. NPP may therefore be temporally and spatially variable. Coastal upwelling off central Chile has been relatively well documented with regards to the hydrological properties and dynamics of upwelling waters (Montecino et al., 2006; Escribano and Schneider, 2007; Kämpf and Chapman, 2016). Additionally, biological properties (such as Chlorophyll-a distribution) and their roles in determining productivity have been investigated (Montero et al., 2007; Iriarte et al., 2012). However, a significant gap remains for understanding temporal NPP dynamics and rates, which in turn limits the knowledge of how NPP rates and their variability are maintained. Information on marine primary production has been centrally important in understanding the fluxes of energy and organic matter in the ocean and the major biogeochemical cycles (e.g., C, N, P).

NPP measurements off the Chilean coast have been performed using different techniques, including O_2, ^{14}C and ^{13}C methods (Montecino et al., 1998; Daneri et al., 2000; Farías et al., 2009; Iriarte et al., 2012). Volumetric primary production rates have been derived from different methods, each one with intrinsic assumptions and biases, which lead to differences in these measurements (Cullen, 2001; Regaudie-de-Gioux et al., 2014). The oxygen evolution (light and dark incubation) method was one of the first techniques capable of determining gross primary production (GPP) and has been widely applied due to its simplicity. However, the ^{14}C method (Steeman Nielsen, 1952) rapidly became the standard for the oceanographic community, and has been used to calibrate remote sensing algorithms (Behrenfeld and Falkowski, 1997a; Banse, 2002). This method was used to measure net primary production NPP, but has been gradually replaced by the use of stable isotope additions, including ^{13}C (Slawyk et al., 1977) and ^{18}O (Bender et al., 1987). The highest primary production estimates are derived using the ^{18}O addition method, while ^{13}C likely underestimates NPP rates, at least as compared to ^{14}C (Regaudie-de-Gioux et al., 2014).

In addition, advances in optical satellite technology over the last three decades have facilitated semi real-time estimations of global NPP (total and fractioned) using multiple models (e.g., Behrenfeld and Falkowski, 1997b; Behrenfeld et al., 2005; Hirata et al., 2009). Despite rich biological productivity (2.57 million tons in 2012 according to FAO, 2014), both measured and estimated NPP rates along Chile's continental shelf are few and discontinuous (i.e., see Table 1 in Thiel et al., 2007) and therefore warrant an effort to combine these approaches.

Different temporal variability in coastal upwelling affects NPP along Chile's coast. As upwelling process occurs, subsurface water of equatorial origin (Equatorial SubSurface Water, ESSW) is upwelled to the surface, delivering waters with low temperature and dissolved O_2 levels, but high salinity and nutrient content (Silva et al., 2009). Areas characterized by a semi-permanent upwelling (off Coquimbo, 30°S) show similar NPP rates throughout the year, while off central Chile (Concepción, 36°S) strong seasonal variability is observed (i.e., Table 1 in Thiel et al., 2007).

Off central Chile, upwelling events are mainly driven by South Pacific Subtropical Anticyclone seasonal fluctuations (Fuenzalida et al., 2008) that promote local southern winds concentrated in spring and summer (Sobarzo and Djurfeldt, 2004) and even synoptic variability with 3–12 day fluctuations leading active and relaxed upwelling events (Aguirre et al., 2014). In addition, upwelling events driven by the Biobío canyon (Sobarzo and Djurfeldt, 2004; Sobarzo et al., 2016) have been documented, as well as NPP enhancement due to the effect of geomorphological protection (Montecino et al., 2006; Henríquez et al., 2007).

The coastal area off Concepción is also influenced by river runoff, mainly from the Itata and Biobío rivers (Saldías et al., 2012; **Figure 1**). Seasonal freshwater discharge to the continental shelf (with a peak during the rainy June and July; Sobarzo et al., 2007) may affect the stability/stratification of the water column, as river runoff mainly affects salinity and coastal NPP with the input of substantial amounts of inorganic nutrients (Sánchez et al., 2008).

Furthermore, remote equatorial processes (i.e., El Niño Southern Oscillation, ENSO) affect the productivity and composition of the marine phytoplankton community in the northern Chile, resulting in a shift in thermocline depth and upwelling patterns (Ulloa et al., 2001; Escribano et al., 2004; Iriarte and González, 2004). The factors affecting NPP off central Chile and the effect of processes such as the ENSO cycle (El Niño (EN) and La Niña (LN) events) on the upwelling and the precipitation regime are poorly understood (Montecinos and Aceituno, 2003; Montecinos and Gomez, 2010), and information regarding biological productivity and phytoplankton phenology remains lacking (Corredor-Acosta et al., 2015).

This study investigates how upwelling events, river runoff, ENSO forcing, and other processes modulate NPP patterns in an upwelling region off Central Chile, using *in situ* NPP measurements and satellite estimated NPP rates. Bio-oceanographic data from the *Centro de Investigación Oceanográfica en el Pacífico Sur-Oriental* (COPAS) time series station, *in situ* NPP measurements from 2006 to 2013, and a decade's worth (2006–2015) of satellite NPP estimations (NPPE), were collected, calibrated and compared in order to infer the mechanisms that cause temporal variability in NPP off central Chile. In this way, this study represents one of the first temporal baselines registering mid-term NPP dynamics and will increase our understanding of how natural and anthropogenic changes in costal upwelling affect C, N and other biogeochemical cycles. Climate change is expected to contribute to a reduction in precipitation in central-south Chile with a concomitant decrease in freshwater discharge (Boiser et al., 2016), and to an increase of along coast winds, which will support upwelling off the coast of central Chile (Sydeman et al., 2014). These climate change scenarios and their impacts (some already observable) may affect NPP rates and timing. Consequently, we may observe alterations in the production of organic carbon and the trophic network, and therefore in heterotrophic organisms and fisheries (Neira and Arancibia, 2004), as well as changes to the magnitude of

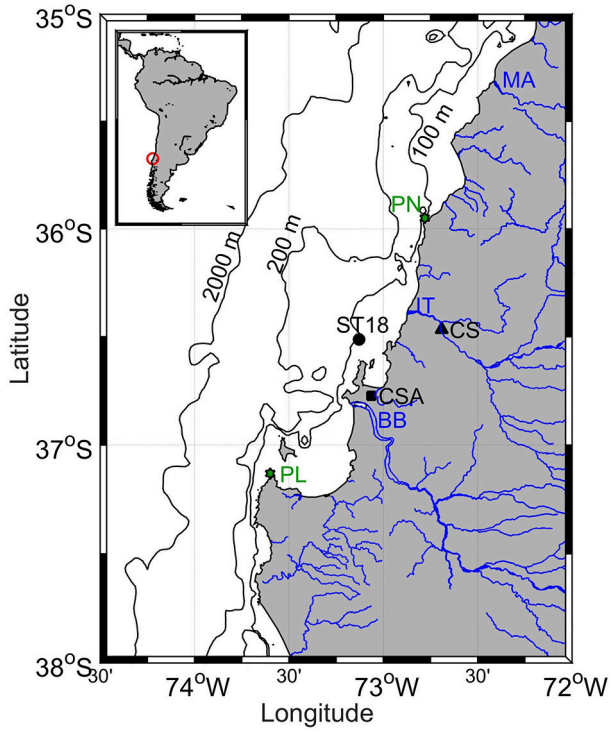

FIGURE 1 | Geographic location of Station 18 (ST18), Coelemu Station (CS), Carriel Sur Airport (CSA), Punta Nugurne (PN), Punta Lavapié (PL), Itata (IT), Biobío (BB), and Maule (MA) rivers. In addition 100, 200, and 2,000 m isobaths are shown.

greenhouse gas exchanges across the air-sea interface (Nevison et al., 2004; Cai et al., 2006).

MATERIALS AND METHODS

Study Zone and Sampling Strategy

The study area is located on the widest (approximately 60 km) continental shelf of Chile (excluding Patagonia) and framed by two submarine canyons (**Figure 1**), formed by the Itata and Biobío (Sobarzo and Djurfeldt, 2004). The area between 35 and 37°S is characterized by an upwelling front ∼25 km wide (Pizarro, 1999). The location of the upwelling front in relation to the coastline is dependent on the position of the major upwelling centers, Punta Nugurne (35°57′S) and Punta Lavapié (37°08′S; **Figure 1**), the width of the continental shelf, and the presence of eddies, filaments, meanders and coastal jet (Sobarzo and Djurfeldt, 2004; Letelier et al., 2009).

In situ observations from January 2006 to January 2016 were provided by the COPAS time series station (ST18), located at the center of the continental shelf, ∼18 nm from shore and a depth of 90 m (**Figure 1**). Monthly cruises (R/V Kay-Kay II) visited the site to collect continuous (temperature, salinity and Photosynthetically Active Radiation, PAR) profiles using a Conductivity Temperature Depth (CTD) probe (SeaBird 19 and SeaBird 25), along with discrete samples for O_2, nutrients, Chlorophyll-a (Chl-a) and NPP rates at depths of 2, 5, 10, 15, 20, 30, 40, 50, 65, and 80 m using 10 L Niskin bottles. In addition, estimations were computed for:

Upwelling Index

We computed the Upwelling Index (UI; m^{-3} s^{-1}) as Ekman zonal transport per 1,000 m of coastline (Bakun, 1973), from 2006 to 2015, using Equation (1):

$$UI = \left(\frac{\tau_y}{\rho f}\right) \cdot 1000m \quad (1)$$

where τ_y (Pa; kg m^{-1} s^{-2}) is the mean wind stress meridional component within the box 73–74°W, 36–39°S, ρ represents the mean density of the water column at ST18 (1026.21 kg m^{-3}), and f indicates the Coriolis parameter corresponding to the latitude of ST18 (8.67 $*10^{-5}$ s^{-1}). Daily τ_y data were obtained from the CoastWatch project (http://coastwatch.noaa.gov). In order to generate the 2006–2015 time series, Level 3 (L3) data were extracted from the Quik Scatterometer (QuikSCAT) mission (spatial resolution = 0.125°) for 1 January 2006 to18 November 2009, and L3 Metop Advanced Scatterometer (ASCAT) data (spatial resolution = 0.25°) was used for 19 November 2009 to 31 December 2015. We estimated a coefficient of determination (r^2) of 0.85, $p < 0.05$ (Fisher's p-value), observed during a period when two satellites overlapped (10 October 2009 until 18 November 2009; y-intercept: 0.0123 and slope: 0.8618).

Monthly standardized anomalies were calculated using Equation (2):

$$Anomaly = \frac{(xN - XN)}{\sigma N} \quad (2)$$

where xN is the discrete value at a certain time, XN is the mean climatological value and σN represents the climatological standard deviation.

Rivers Runoff and Precipitation Rates

Data for Itata River daily runoff were collected at the Coelemu Station (72°41′W, 36°28′S), and daily rainfall was recorded at a meteorological station at the Carriel Sur Airport (73°4′W, 36°46′S, **Figure 1**). Both datasets were provided by the Chilean *Dirección General de Aguas* (DGA; http://www.dga.cl/).

Oceanic Niño Index

ENSO was measured as the Oceanic Niño Index (ONI); data were obtained from the Climate Prediction Center (http://www.cpc.ncep.noaa.gov/). For cumulative analysis and considering that data did not cover the entire period of EN 2015-16, five EN and LN events were selected. We used Monte Carlo experiment (1,000 iterations) to assess statistical significance between cumulative NPPE during EN and LN events (Montecinos and Gomez, 2010).

Net Primary Production Estimations

NPPE were obtained using the standard Vertically Generalized Production Model (VGPM; Behrenfeld and Falkowski, 1997b) and extracted using 8-day average estimations at a spatial resolution of ∼9 km (Ocean Productivity Page, http://www.science.oregonstate.edu/ocean.productivity/). Among many

TABLE 1 | Summary of error statistics, i.e., Absolute Average Error (AAE), Root Mean Square Error (RMSE), Bias Mean Normalized Bias (P_{BIAS}), Mean Absolute Percentage Error (MPE) and r^2 coefficients for different satellite NPP areas.

Matrix dimensions (lon × lat)	Comments	*n*	AAE	RMSE	Bias	P_{BIAS} (%)	MPE (%)	r^2
1 × 1	*In situ* measurements	54	/	/	/	/	/	/
1 × 1	Pixel nearest to ST18	54	3.66	4.80	3.17	153.60	673.21	0.47
2 × 2	Avg of the 4 pixels nearest to ST18	54	3.35	4.40	2.73	132.15	619.00	0.51
3 × 3	Pixel nearest to ST18 in the center of the grid	54	3.33	4.27	2.75	133.22	620.52	0.56
5 × 5	″	54	3.07	3.95	2.45	118.69	594.08	0.57
7 × 7	″	54	2.85	3.62	2.20	106.41	578.06	0.58
9 × 9	″	54	2.66	3.37	1.98	95.80	561.85	0.58
11 × 11	″	54	2.47	3.14	1.73	83.63	546.15	0.58
13 × 13	″	54	2.33	2.97	1.48	71.80	531.21	0.59
15 × 13	74°-72°45′ W, 36°-37° S	54	2.02	2.75	0.89	43.31	462.99	0.61

NPP models, standard VGPM from SeaWiFS was considered as the model with higher correlation ($r^2 = 0.66$) with 610 *in situ* NPP measurements calculated for the California Current (Kahru et al., 2009).

In order to obtain representative satellite estimates, a NPPE time series was created with 8-day average estimations for a similar time period as used for *in situ* measurements. Next, basic statistics parameters were used to compare *in situ*-satellite data for different pixel boxes (Swirgon and Stramska, 2015). Comparison revealed higher correlation between NPP and NPPE, expressed as r^2, and lower error, within the boundaries of 72°45′-74°W, 36–37°S (**Table 1**), a zone with a total area of $13*10^3$ km^2 and approximately 55% located over the continental shelf. Analysis of variance (ANOVA) and linear regressions were performed using model II reduced major axis regression (Legendre and Legendre, 1998). Mean values for each pixel box were calculated, except in the case of the pixel box nearest to ST18, which used a single estimation. If a mean estimation described at least 33% of the pixels, it was considered valid.

NPPE Weekly Variability

The magnitude of week-to-week (WW) NPPE variability was calculated using Equation (3):

$$WW = w_t - w_{(t+1)} \quad (3)$$

where w_t represents the 8-day-average NPPE during time t and $w_{(t+1)}$ is the successive NPPE.

Wavelet analysis was used to establish dominant frequency bands and their recurrence in the time series, decomposing the signal and estimating its spectral characteristics as a function of time (Torrence and Compo, 1998). Continuous Morlet wavelet transform was applied using the MATLAB functions provided by Torrence and Compo (1998; http://paos.colorado.edu/research/wavelets).

Agglomerative hierarchical cluster analysis (single linkage technique) was used to evaluate the degree of dissimilarity in monthly bio-oceanographic features.

Photosynthetically Active Radiation

L3 satellite PAR data were obtained (using 8-day composites with a spatial resolution of ∼4 km) from the Aqua Moderate Resolution Imagining Spectroradiometer (MODIS) mission, within the limits 72–76°W and 35–39°S. Photic Layer Depth (PLD) was estimated using 62 *in situ* instant PAR profiles collected using a Biospherical QSP 2150 sensor deployed together with CTD profiler. PLD was identified as the depth where downwelling photosynthetic photon flux was equal to 1% of the surface value. Satellite-determined PLD was calculated as PLD = $\ln(0.01)*K_{490}^{-1}$ (Behrenfeld et al., 2005), using the 8-day composite Diffuse Attenuation Coefficient K_{490} (with a spatial resolution of 4 km) from the Aqua MODIS mission. The vertical attenuation coefficient for downward irradiance in the upper 20 m was calculated as described by Kirk (1983).

Phytoplankton Sizes Classes

Calculations from Hirata et al. (2011) were used to estimate the percentage contribution of micro-, nano- and picophytoplankton to total satellite Chl-a estimations. L3 MODIS Chl-a estimations (8-day average at a spatial resolution of 4 km) were analyzed for the area 72°45′-74°W, 36–37°S by setting the proportions of microphytoplankton >100% at 100%, and negative proportion of picophytoplankton at 0%.

Net Primary Production Measurements

A total of 54 *in situ* NPP monthly measurements were obtained from July 2006 to December 2013 at ST18 (**Figure 1**). At least four measurements for the photic layer are available for every month, with 5–9 monthly measurements available from 2008 to 2013. Light Carbon Assimilations Rates (LCAR) were calculated using the ^{13}C stable isotopic technique (Slawyk et al., 1977) on a mooring line. Samples were captured in polycarbonate 0.6 L bottles, starting at the surface and to a maximum depth of 50 m. The ^{13}C tracer concentration was 3.6456 mg ^{13}C mL^{-1}, equivalent to 0.5 mmol mL^{-1}, and 0.5 mL of tracer was added to each sample, to achieve approximately 10% enrichment. Immediately following tracer addition and prior to sunrise, bottles were deployed to sampling depths for *in situ* incubation.

Incubation periods of 10–12 h (counted from the time of sunrise) were used to average phytoplankton physiological activities along the day. Incubation was terminated at dusk using gentle vacuum filtration (<100 mm Hg) through precombusted grade GF/F glass filters. Filters were dried at 60°C for 24 h and then stored at constant temperature until laboratory analysis using continuous-flow isotope ratio mass spectrometry (Finnigan Delta Plus IRMS).

NPP rates were determined as LCAR (mg C m^{-3} t^{-1}) (Raimbault et al., 1999; Fernández et al., 2005) according to Equation (4):

$$\rho DI^{13}C = \left[\frac{(\%R_{POC} - R_n) * \left(\frac{POC}{12 * V_f} \right)}{\%R_{DIC}} \right] * 12 \quad (4)$$

$$\%R_{DIC} = \frac{\left(\frac{V^{13}C * {}^{13}DIC}{V_b} \right) + DIC_i * 0.01112}{DIC_i - \frac{V^{13}C * {}^{13}DIC}{V_b}} * 100 \quad (5)$$

where V_f represents filtered volume and *POC* is the amount of particulate organic carbon recovered in the filter after incubation and measured by mass spectrometry (μg). The excess enrichment of the tracer after inoculation (To) is indicated by $\%R_{DIC}$, calculated using Equation (5). $\%R_{POC}$ indicates ^{13}C enrichment in the filter after incubation, measured by the tracer mass. In Equation (5), $V^{13}C$ indicates the volume of ^{13}C added to the sample during the inoculation, while ^{13}DIC accounts for the tracer concentration added to the sample (3.6456 mg ^{13}C mL^{-1}). DIC_i represents the initial amount of dissolved inorganic carbon in the sample before inoculation. For this study, a constant value of 26 mg C L^{-1} was selected and applied based on previous measurements for the area (Paulmier, unpublished data). V_b is the volume in the incubation flask (0.6 L). Volumetric assimilation rates (LCAR) were integrated for the photic layer throughout the photoperiod in order to estimate integrated NPP rates (g C m^{-2} d^{-1}). In this way, our measurements do not include dark respiration, which may cause overestimation of NPP rates (Regaudie-de-Gioux et al., 2014).

Physico-chemical Variables

Brunt-Väisälä frequency (BVF) based on temperature and salinity data were obtained using the Ocean Data Viewer (version 4.7.4). Dissolved oxygen was analyzed in triplicate for a 125 mL sample by Winkler titration using a Dosimat 665 with automatic photometric end-point detector (detection limit ∼2 μmol L^{-1}). Fixed samples were analyzed between 12 and 24 h after collection and the percent saturation of dissolved oxygen was calculated based on Boyer et al. (1999).

Triplicate samples for nutrients were filtered onboard (using 0.7 μm, grade GF-F glass filters for NO_3^- and PO_4^{3-} and 0.45 μm membrane of cellulose acetate for $Si(OH)_4$, stored in 15 mL screw-capped centrifuge tubes, and frozen (at −20°C) until analysis. Until 2011, nutrient concentrations were determined using standard manual colorimetric techniques (Grasshoff et al., 1983) and *a posteriori* using the Seal AutoAnalyzer 3 (AA3). We only considered $Si(OH)_4$ data from 2010 to 2016 because of possible contamination due to sampling strategy during the period 2006–2009. Chl-a was measured for triplicate 250 mL water samples, filtered using 0.7 μm, grade GF/F glass fiber filters. Samples were frozen at −20°C and later analyzed using fluorometry (Turner Designs 10AU^{TM}) according to standard procedures (Parsons et al., 1984).

Upwelling-Driven Nutrient Flux

Upwelling-driven nutrient flux (kmol d^{-1}; with 1 kmol = 10^3 mol) from 2003 to 2016 was calculated according to Equation (6):

$$F = UI \cdot C \quad (6)$$

where *UI* is the mean upwelling index (m^3 s^{-1}) during the 3 days prior to field survey and C represents the mean concentration of subsurface nutrients (40–80 m; mmol m^{-3}) at ST18. *UI* was calculated as volumetric Ekman zonal transport per 1,000 m of coastline; explained by the width of the Itata River mouth (∼1,000 m) and our goal of comparing the two fluxes over an area of similar order of magnitude. This simple model assumes: (1) a constant wind field with no changes in magnitude and direction (i.e., without considering wind curl and Ekman pumping); (2) an ocean with no horizontal or vertical boundaries (i.e., ignoring upwelling events induced by topography and trapped waves); (3) the replacement of the zonal transport by vertical advection (i.e., without considering horizontal advection); (4) an absence of diapycnal mixing; and 5. downwelling-favorable winds produce nutrient loss from the photic layer.

Nutrient Export by River Discharge

Nutrient flux (kmol d^{-1}) from Itata River discharge between 2003 and 2016 was calculated using Equation (7):

$$F = Q \cdot C \quad (7)$$

where *Q* represents mean Itata runoff (m^3 s^{-1}) during the 3 days prior to field survey and *C* is the nutrient concentration (mol m^{-3}) at the Coelemu station (**Figure 1**). Approximately trimonthly NO_3^- and PO_4^{3-} concentrations were obtained from the DGA; NO_3^- was estimated using Kjeldahl methods; PO_4^{3-} was determined colorimetrically by spectrophotometry. In the absence of $Si(OH)_4$ measurements in the Coelemu station dataset, a well-established stoichiometric ratio, $Si(OH)_4$:NO_3^- = 7.745 (μM/μM; Yévenes, personal communication), was used to estimate $Si(OH)_4$ concentrations from existing NO_3^- data in the Itata River. Our simple approach attempted to compare nutrient input from wind-driven coastal upwelling (NO_3^-, PO_4^{3-} and $Si(OH)_4$) and from river discharge (freshwater source) in the study zone.

RESULTS

Annual Cycles and Their Interannual Variability

Meteorological and Hydrological Forcing Agents

From 2006 to 2015, the upwelling index (UI) oscillated between −3,324 and 4,369 m^3 s^{-1} 1,000 m^{-1} coastline (**Table 2**; Supplementary Figure 1).The annual cycle based on monthly

TABLE 2 | Summary of statistics values, i.e., number of samples (n), Minimum (Min), Maximum (Max), Mean and Standard Deviation (SD) for variables analyzed in annual cycles section. *In situ* mean values were calculated for the upper 10 m of the water column.

	n	Min	Max	Mean ± *SD*
METEOROLOGICAL AND HYDROLOGICAL FORCING AGENTS				
Upwelling Index [m^3 s^{-1} 1,000 m^{-1}]$^{\Phi}$	3,591	−3,324	4,369	646 ± 940
Itata Runoff [m^3 s^{-1}]	3,408	13.2	4,242	282.2 ± 347.8
Rain Rate [mm d^{-1}]	3,648	0	112.5	2.9 ± 8.8
Surface PAR [E m^{-2} d^{-1}]$^{\Phi}$	457	9.45	66.87	37.9 ± 16.6
OCEANOGRAPHIC VARIABLES				
Temperature [°C]	112	10.6	16.7	12.7 ± 1.2
Salinity	112	26.9	34.8	33.8 ± 1.2
Brunt-Vaisala Frecuency [cycl h^{-1}]	112	−17.9	57.7	8.0 ± 10.2
Oxygen [μM]	87	119.5	338.7	249.8 ± 43.5
Nitrate [μM]	107	0.3	28.1	11.3 ± 6.1
Upwelling Nitrate Flux [kmol d^{-1}]	140	−2152.2	6953.3	1470.6 ± 1769.9
Continental Nitrate Flux [kmol d^{-1}]	34	2.7	691.4	110.2 ± 153.1
Phosphate [μM]	107	0.1	2.8	1.4 ± 0.5
Upwelling Phosphate Flux [kmol d^{-1}]	140	−212.7	756.2	169.2 ± 193.3
Continental Phosphate Flux [kmol d^{-1}]	39	0.1	55.3	9.9 ± 11.0
Silicate [μM]	57	0.2	20.4	7.9 ± 5.3
Upwelling Silicate Flux [kmol d^{-1}]	59	−2927.8	6550.0	1352.0 ± 1753.6
Continental Silicate Flux [kmol d^{-1}]	34	20.9	5355.2	853.1 ± 1186.1
PHOTIC LAYER, CHLOROPHYLL-A AND PRIMARY PRODUCTION RATES				
Photic Layer depth [m]	58	7	49	23.8 ± 11.9
Photic Layer depth [m]$^{\Phi}$	440	6.7	61.6	32.3 ± 9.6
Chlorophyll-a [mg m^{-3}]	703	0.0	53.1	2.48 ± 5.83
Surface Chlorophyll [mg m^{-3}]	83	0.1	36.1	4.7 ± 7.2
Surface Chlorophyll [mg m^{-3}]$^{\Phi}$	450	0.4	18.6	4.1 ± 3.4
Microphytoplankton [% Chl-a]$^{\Phi}$	450	18.3	96.5	60.1 ± 13.6
Nanophytoplankton [% Chl-a]$^{\Phi}$	450	2.9	49.4	23.6 ± 7.9
Picophytoplankton [% Chl-a]$^{\Phi}$	450	0.5	32.3	16.3 ± 5.7
LCAR [g C m^{-3} d^{-1}]	216	0.2	1721.7	74.0 ± 207.7
NPP [g C m^{-2} d^{-1}]	54	0.03	18.23	2.06 ± 3.12
NPPE [g C m^{-2} d^{-1}]$^{\Phi}$	454	0.45	9.07	2.97 ± 1.69

$^{\Phi}$*indicates satellite estimation.*

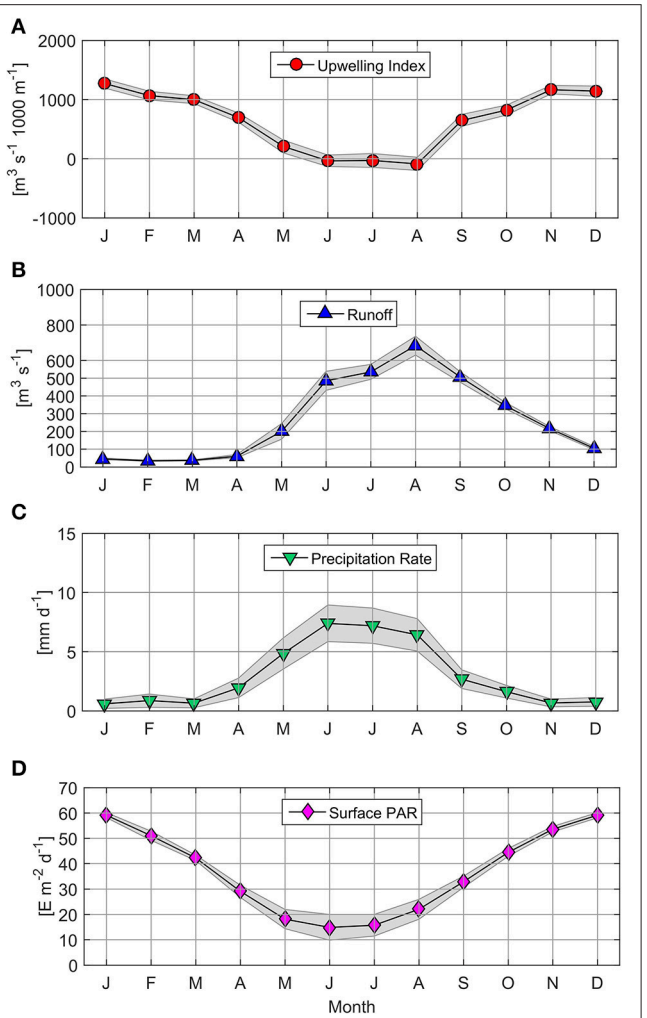

FIGURE 2 | Mean climatology for Upwelling Index **(A)**, Itata Runoff **(B)**, Precipitation Rate **(C)**, and Surface PAR **(D)**. Markers indicate monthly mean values; the shaded area represents monthly 95% confidence interval.

averages of UI time series revealed the predominance of upwelling favorable winds from September to April (66% of the year, with a maximum monthly mean of 1,271 m^3 s^{-1} 1,000 m^{-1} in January; see **Figure 2A**). By contrast, downwelling-favorable winds dominated between June and August and produced a negative UI value with a monthly mean of −87 m^3 s^{-1} 1,000 m^{-1} during August.

High Itata River runoff (>400 m^3 s^{-1}) was observed from June to September, with a maximum monthly mean of 683 m^3 s^{-1} during August (**Figure 2B**). River discharges of less than 60 m^3 s^{-1} were observed between January and April. The majority of Itata River runoff was explained by precipitation ($r^2 = 0.33$, $p < 0.05$, $n = 418$; **Figure 2C**).

Satellite surface PAR estimations (monthly means) were highest from November to February (>50 E m^{-2} d^{-1}; **Figure 2D**), and lowest (between 14.89 and 22.05 E m^{-2} d^{-1}) from May to August.

Oceanographic Variables

Temperature presented a clear seasonal variation (**Figure 3A**). From December to March, when a warming of the thin surface layer (with values higher than 13°C), caused by high levels of short wave radiation contrasted with the upwelling of cool subsurface water from the ESSW, created a marked thermal stratification. The intrusion of cold ESSW advected by coastal upwelling and demarked by an 11.2°C isotherm was clearly observed from September to March, due to a favorable upwelling process (**Figure 3A**). Between May and August the water column presented fairly homogeneous conditions, with higher temperatures with respect to upwelling periods mainly associated with Subantarctic Water (SAAW; Silva et al., 2009).

Seasonal variation in salinity was also observed (**Figure 3B**). Low salinity was detected in a thin surface layer each winter and spring and coincided with high precipitation and river runoff. From June to October, a low salinity area associated with the Itata River plume often extended as far as the zone around ST18, creating notable haline stratification (**Figure 3B**). During 2014 and 2015, the lowest salinities were also observed in the spring (i.e., 20.34 in November 2014 and 25.70 in October

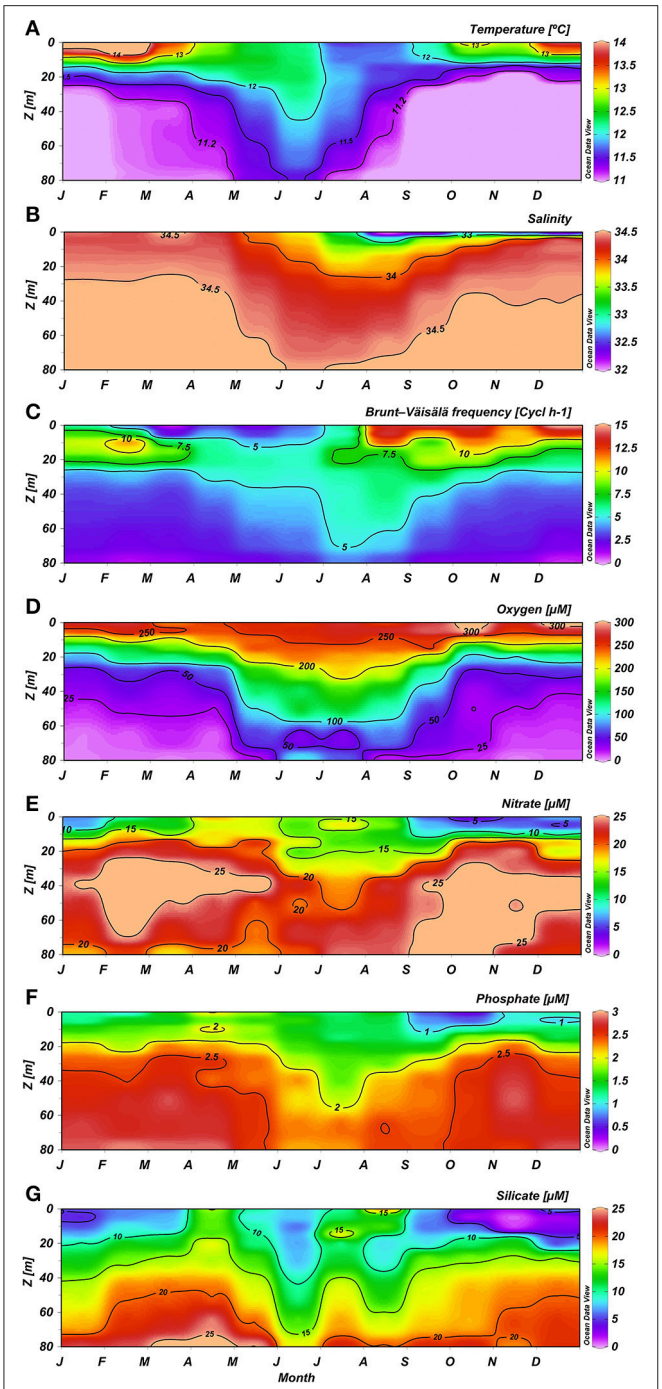

FIGURE 3 | Mean climatology for Temperature **(A)**, Salinity **(B)**, Brunt-Väisälä frequency **(C)**, Oxygen **(D)**, Nitrate **(E)**, Phosphate **(F)**, and Silicate **(G)** at ST18.

2015; Supplementary Figure 2). Salinity ≥34.0 was observed for the upper 20 m of the water column from June to September, with intermediate surface riverine influence between October and December, and sporadic events from January to April. Higher BVF values were observed between depths of 0 and 20 m, particularly from August to December (**Figure 3C**), and likely due to river discharge; subsurface BVF values appeared to be mainly associated with thermal stratification throughout the year, with the exception of late autumn (April and May). Upwelling of the nearly-homogenous ESSW between October and May caused high density homogeneity and lower BVF values between 30 and 80 m. During austral winter, however, elevated deep stability was observed.

Oxygen distribution in the water column (**Figure 3D**) presented higher O_2 concentrations (>200 µM) in the upper 15–20 m depth throughout the entire year, but subsurface water exhibited seasonal variation due to the intrusion of poorly-oxygenated ESSW from coastal upwelling. Subsurface hypoxic waters (with O_2 levels lower than 50 µM) were observable during the upwelling season from September to April; while between May and August this layer was deeper and more oxygenated (**Figure 3D**).

The surface layer showed reduced but not depleted nutrient concentrations, whereas the subsurface layer presented consistently higher nutrient concentrations (**Figures 3E–G**). Within the upper 10 m, NO_3^- and PO_4^{3-} showed minimum mean concentrations from September to January (with minimums of 6.66 and 0.75 µM in October, respectively), intermediate values in wintertime (at 13.74 and 1.41 µM in August, respectively) and higher values between February and May (with maximums of 17.46 and 1.96 µM, respectively, observed in April). These trends were consistent with the plankton temporal dynamics (see below). In contrast, $Si(OH)_4$ exhibited higher concentrations during late autumn and winter, and lower values (with a minimum mean value of 2.13 µM in November) during spring and summer (**Figure 3G**). This pattern reflects the high levels of $Si(OH)_4$ associated with river discharge and the development of diatom blooms in spring and summer.

Mean upwelling-driven NO_3^- and PO_4^{3-} fluxes were an order of magnitude higher than continental discharges from Itata River (**Table 2**). Conversely, mean oceanic $Si(OH)_4$ flux (1,352 kmol d^{-1}) was comparable to river input (853 kmol d^{-1}). High standard deviation was partially explained by seasonal variability (**Figure 4**). Indeed, wind-driver nutrient flux was higher from September to April (>1,086, 141, and 1,041 kmol d^{-1} for NO_3^-, PO_4^{3-} and $Si(OH)_4$, respectively), as compared with the rest of the year, whereas continental inputs reached maximum values between June and August (>226, 15, and 1,755 kmol d^{-1} for NO_3^-, PO_4^{3-} and $Si(OH)_4$, respectively).

Photic Layer, Chlorophyll-a and Primary Production Rates

Light penetration varied temporally, with a higher vertical attenuation coefficient (0.22 m^{-1}) from October to January, as compared with February to April (0.18 m^{-1}) and June to August (0.12 m^{-1}). In this way, PLD showed a distinctive seasonal pattern, with deepening in winter (to approximately 35 m) as compared to ∼15 m during spring-summer, and intermediate values during late summer-autumn (∼25 m, **Figure 5A**). Climatology for satellite-derived PLD revealed a similar temporal pattern (deeper values from April to August) as compared to *in situ* measurements (**Figure 5A**), although satellite estimations appeared to overestimate PLD, especially from September to February and in May.

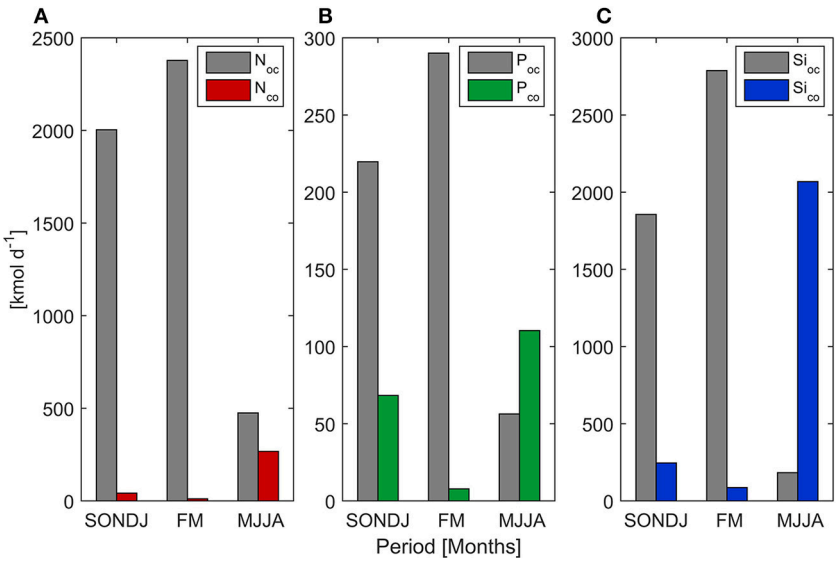

FIGURE 4 | Mean value of Nitrate **(A)**, Phosphate **(B)**, and Silicate **(C)** flux from upwelling ($_{oc}$) and river discharge ($_{co}$) during three periods of the year.

In situ Chl-a concentrations higher than 1 mg m^{-3} (with a marked subsurface peak through variable depths) were observed from September to May within the upper 20 m of the water column, while lower and more homogeneous values (ranging from 0.5 to 1 mg m^{-3}) were detected during winter (**Figure 5B**). Maximum monthly means of surface Chl-a were observed during October (12.0 mg m^{-3}), with minimum values (of 0.85 mg m^{-3}) recorded in July. The highest monthly mean of satellite Chl-a (7.7 mg m^{-3}) was registered during December (**Figure 5C**), while the lowest monthly mean (1.4 mg m^{-3}) was observed in July.

Microphytoplankton contributed between 18.3 and 96.5% of Chl-a, with the greatest overall contribution to total Chl-a observed during spring-summer (October–January), with monthly mean contributions from 65.5 to 69.2% (**Figure 5D**). The largest phytoplankton size class demonstrated elevated values from February to April (59.1–66.9% Chl-a), decreasing to below 50% in winter. Throughout the annual cycle, the nanophytoplankton community made greater contributions to Chl-a than picophytoplankton, with highest monthly means recorded in July (31.3 and 22.3% Chl-a, respectively).

Throughout the year, LCAR was greater than 20 mg C m^{-3} d^{-1} in the surface layer; LCAR greater than 100 mg C m^{-3} d^{-1} was observed during the entire upwelling season (**Figure 5E**). LCAR greater than 400 mg C m^{-3} d^{-1} was observed in surface waters (5–10 m depth) in spring and early summer (October 2006, December 2007, January, September and November 2009, and January 2011 and 2013; Supplementary Figure 3), and exceptionally high values of 1,721 and 1,536 mg C m^{-3} d^{-1} were recorded during November 2006 and 2013 at a 5 m depth, indicating NPP hotspots. Excluding the exceptionally high LCAR event in November 2006, LCAR:Chl-a mean values of 19.5 and 31.8 mg C mg Chl-a^{-1} d^{-1} were obtained for non-favorable and favorable upwelling periods, respectively, indicating that the wintertime phytoplankton community presents comparable photosynthetic efficiency with groups characterizing the upwelling season.

Daily integrated LCAR for the photic layer varied between 0.03 and 18.23 g C m^{-2} d^{-1}. NPP measurements showed a clear seasonal cycle, with lower monthly mean from February to August (from 0.22 to 1.81 g C m^{-2} d^{-1}, **Figure 5F**) as compared to September-January (1.81 to 6.43 g C m^{-2} d^{-1}). Monthly winter averages between 0.24 (July) and 0.84 g C m^{-2} d^{-1} (August) were observed.

Satellite NPPE fluctuated from 0.45 to 9.07 g C m^{-2} d^{-1} with the same seasonal variability as observed for Chl-a (**Figure 5F**). Between October and January, NPPE were higher than 3.9 g C m^{-2} d^{-1} (with a maximum monthly mean of 5.1 g C m^{-2} d^{-1} in December), while from February to June NPPE decreased to 1.1 g C m^{-2} d^{-1}. Basal productivity between 1.1 and 1.5 g C m^{-2} d^{-1} was observed using satellite estimations during the winter season. In September, mean NPPE rose to 2.9 g C m^{-2} d^{-1} with the activation of upwelling-favorable wind.

A linear regression calculated for *in situ* NPP and integrated Chl-a for the PLD and between satellite NPPE and Chl-a indicated significant determination coefficients of $r^2 = 0.50$ and $r^2 = 0.86$, respectively (**Table 3**). The regression for *in situ* NPP and satellite NPPE data within the limits of 72°45′-74°W and 36–37°S revealed a r^2 of 0.61 (**Table 3**), but when this data were separated into two periods, higher r^2 values were found during winter ($r^2 = 0.70$) with respect to the rest of the year ($r^2 = 0.24$).

The annual NPP cycle off central Chile has been traditionally divided in two oceanographic periods: a favorable and non-favorable upwelling season based on physical (Montecino et al., 2006; Sobarzo et al., 2007) and biological (Morales et al., 2007) criteria. However, when bio-oceanographic processes and variables, such as NPP, PLD and nutrients, are considered, a hierarchical cluster tree with a cophenetic correlation coefficient of 0.83 separates the annual NPP cycle into three

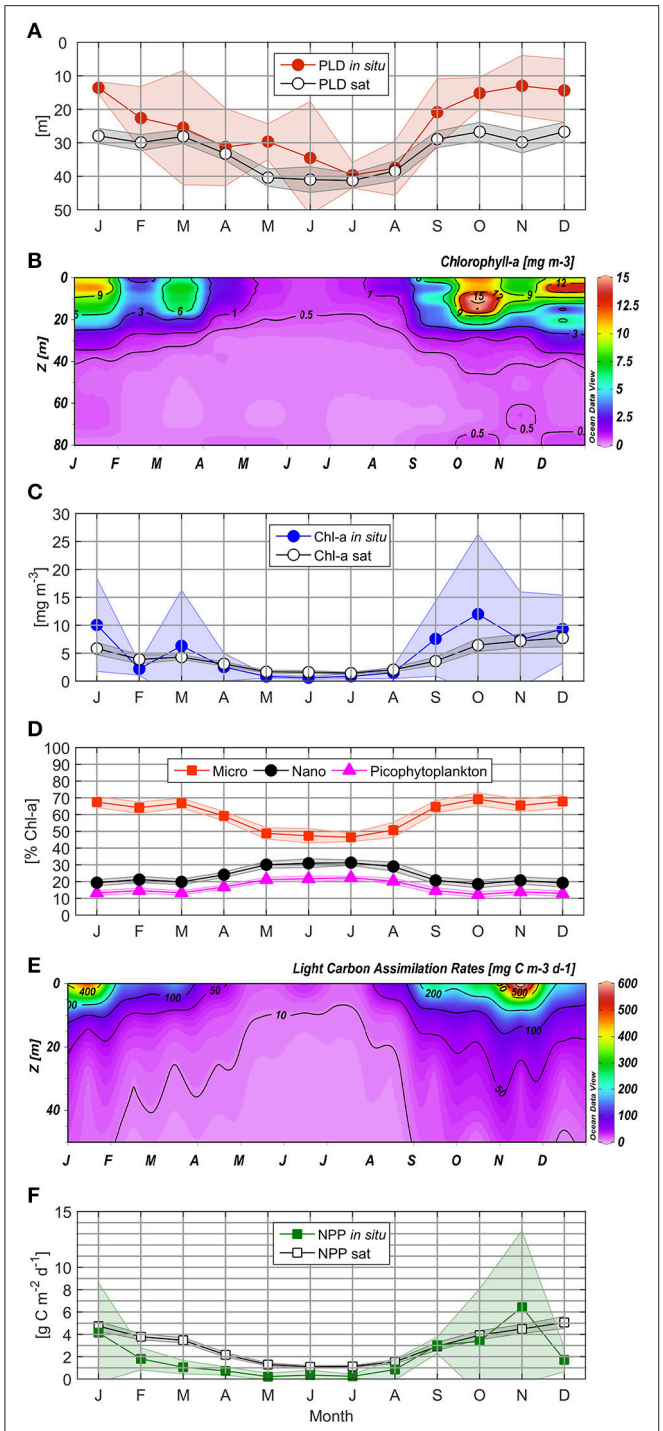

FIGURE 5 | Mean climatology for *in situ* and satellite Photic Layer Depth **(A)**, Chlorophyll-a **(B)**, *in situ* and satellite surface Chlorophyll-a **(C)**, Phytoplankton size classes **(D)**, Light Carbon Assimilation Rates **(E)**, and *in situ* and satellite Net Primary Production **(F)**. Markers indicate monthly mean values; the shaded area indicates monthly 95% confidence interval.

different periods (see **Figure 6**): a rising stage (high NPP), a falling stage (intermediate NPP) and a basal stage (low or basal NPP). The bio-oceanographic features observed for the study area during these periods are summarized in **Table 4**.

TABLE 3 | Summary of error statistics, i.e., number of observations (n), r^2 coefficient, and ANOVA F and *p*-values for biological variables (Chl-a, Chlorophyll-a; NPP, *in situ* Net Primary Production; NPPE, satellite-derived Net Primary Production Estimation).

				ANOVA	
		n	r^2	***F***	***p*-value**
Chl-a* vs. NPP		43	0.50	40.57	<0.001
Chl-a$^{\Phi}$ vs. NPPE		444	0.86	2799.40	<0.001
NPP vs. NPPE	All data	54	0.61	80.54	<0.001
	Upwelling	36	0.24	10.89	<0.001
	Winter	18	0.70	34.72	<0.001

**indicates Chlorophyll-a integrated within the photic layer; $^{\Phi}$indicates satellite estimation. Upwelling period: September to April. Winter: May to August.*

Interannual Variability of NPP and its Relationship With ENSO

We observed three EN (2006–07, 2009–10, 2015–16) and three LN (2007–08, 2010–11, 2011–12) events of varying magnitude and duration between 2006 and 2015 (**Figure 7**). Minimum ONI measurements (−1.4°C) were found during January 2008, October 2010 and December 2010, while maximum ONI indexes (+1.3°C) were observed during December 2009 and January 2010.

Interannual variability in NPPE was also observed, with higher cumulative NPPE during neutral year 2014–15, LN 2010–11, and LN 2011–12 (1.28, 1.21, and 1.15 kg C m^{-2} yr^{-1}, respectively; see **Figure 7C**). In contrast, the lowest values were observed during the neutral years 2012–13 and 2013–14 (0.98 and 1.01 kg C m^{-2} yr^{-1}, respectively). Cumulative NPPE during EN and LN years yielded mean values of 1.07 and 1.14 kg C m^{-2} yr^{-1}, respectively. Mean NPPE was 1.1 kg C m^{-2} yr^{-1}. No statistical significance (Monte Carlo simulations, 1,000 iterations) was determined for NPPE between EN and LN conditions. A NPP wavelet power spectrum and normalized global wavelet spectrum revealed low variance and no statistical significance in interannual variability (**Figure 8**), and identified annual variation as the dominant frequency band.

DISCUSSION

The continental shelf off Concepción is an important upwelling zone and has been described as one of the most productive areas within the Humboldt Current system (Montecino et al., 1998; Montero et al., 2007; Thiel et al., 2007; Daneri et al., 2012; Iriarte et al., 2012). However, no systematic measurements of NPP have been performed, and NPP rates showed a great variability (e.g., 0.1 and 25.8 g C m^{-2} d^{-1}). Understanding the wide variation in NPP rates, NPP dynamics and factors controlling NPP is vital to improve our knowledge of C, N, and P cycles in central Chile.

At 36°S, upwelling occurs over one of the widest continental shelves along the southern part (18–41°S) of Humboldt EBUS. This shelf accelerates benthic pelagic coupling and thus the

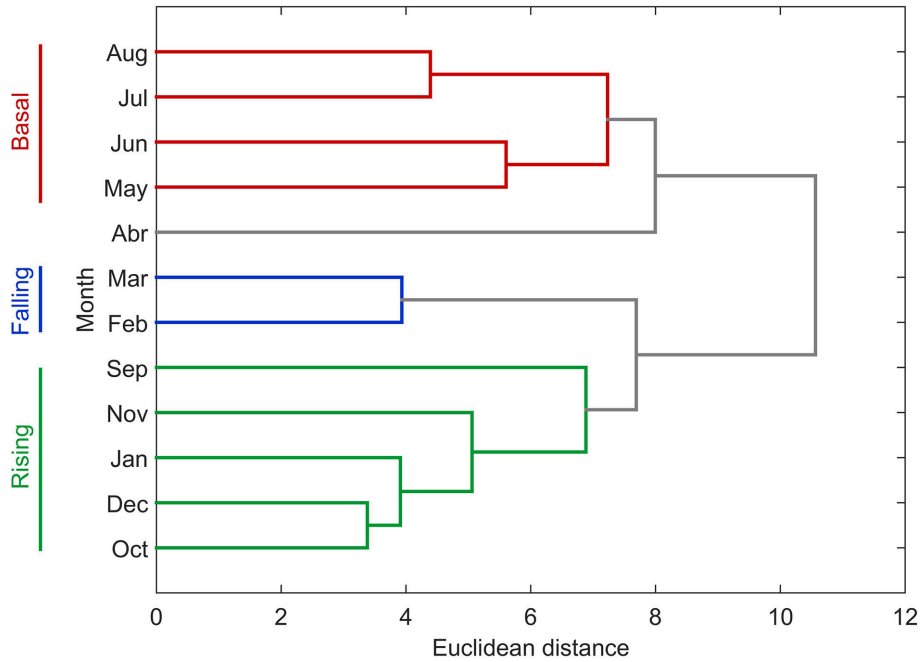

FIGURE 6 | Dendrogram presenting hierarchical clustering of the degree of similarity between monthly bio-oceanographic characteristics. We used monthly mean surface (0–10 m) values for temperature, salinity, nutrients (nitrate, phosphate and silicate) along with monthly means for satellite and *in situ* net primary production, satellite and *in situ* photic layer depth, satellite Chlorophyll-a and upwelling index.

TABLE 4 | Summary of bio-oceanographic conditions during three different periods of the year off central Chile (mean ± standard deviation).

Season	**Rising stage**	**Falling stage**	**Basal stage**
	(High productivity–upwelling activation)	**(Intermediate productivity–upwelling decay)**	**(Basal productivity–wet)**
Months	**September–January**	**February–March**	**May–August**
Upwelling index [m^3 s^{-1} 1,000 m^{-1}]$^{\Phi}$	1008.91 ± 772.75	1030.22 ± 609.94	13.46 ± 976.08
River runoff [m^3 s^{-1}]	249.36 ± 223.06	35.94 ± 25.74	482.04 ± 458.09
Temperature [°C]	12.91 ± 1.37	13.58 ± 1.33	12.02 ± 0.73
Salinity	33.71 ± 2.55	34.41 ± 0.33	33.47 ± 0.95
Brunt-Väisälä frequency [cycl h^{-1}]	10.86 ± 15.31	4.62 ± 8.57	6.83 ± 8.86
Oxygen [μM]	258.26 ± 67.19	236.79 ± 59.15	256.18 ± 30.06
Oxygen saturation (%)	126.25 ± 29.25	115.17 ± 28.75	120.90 ± 20.31
Nitrate [μM]	7.39 ± 7.04	12.91 ± 7.04	14.69 ± 4.95
Phosphate [μM]	1.05 ± 0.61	1.47 ± 0.56	1.48 ± 0.42
Silicate [μM]	4.66 ± 5.23	6.76 ± 3.49	10.52 ± 6.50
Surface PAR [E m^{-2} d^{-1}]$^{\Phi}$	46.55 ± 13.03	50.99 ± 6.44	18.57 ± 4.97
Diffuse attenuation coefficient [m^{-1}]$^{\Phi}$	0.46 ± 0.29	0.31 ± 0.12	0.14 ± 0.05
Photic Layer Depth [m]	15.65 ± 7.59	23.89 ± 9.58	35.82 ± 8.46
Photoperiod [h]	13.68 ± 0.94	12.45 ± 0.58	10.24 ± 0.58
Chlorophyll-a [mg m^{-3}]	9.58 ± 9.01	6.54 ± 12.38	0.90 ± 0.83
Microphytoplankton [% Chl-a]$^{\Phi}$	66.95 ± 11.41	65.71 ± 9.11	48.41 ± 11.37
NPP [g C m^{-2} d^{-1}]	3.98 ± 4.16	1.39 ± 0.69	0.46 ± 0.59

Based on cluster analysis, we considered April as transitional month with high variability. In situ mean values were calculated for the upper 10 m of the water column. $^{\Phi}$*indicates satellite estimations.*

supply of regenerated N, P and even Fe from sediment to bottom water (Farías et al., 1996; Graco et al., 2006; Fennel, 2010), which in turn controls NPP (Ryther and Dunstan, 1971). Thus, the Atlantic EBUS are also characterized by a wider continental shelf and higher NPP as compared to the Pacific, where the Humboldt EBUS presents higher productivity than the California

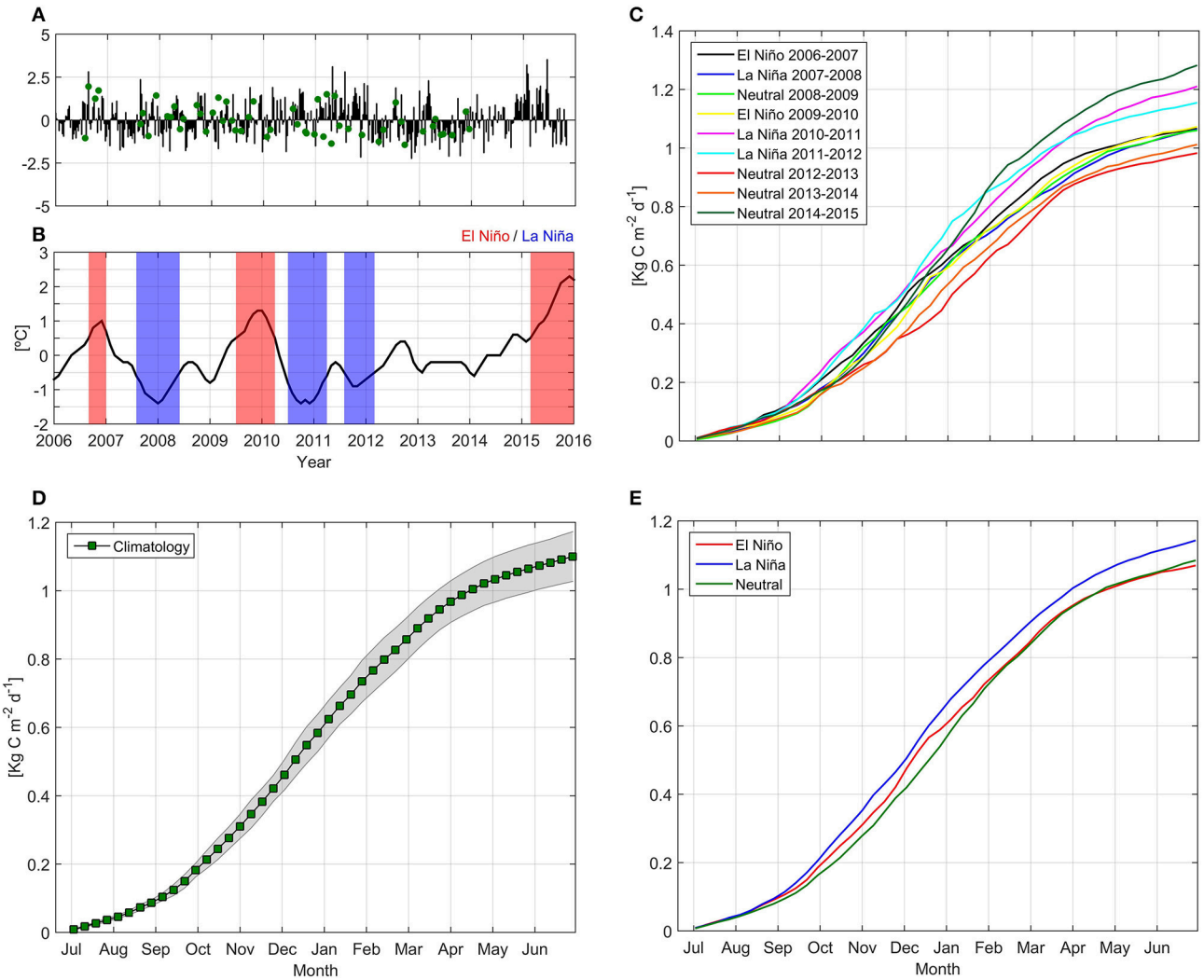

FIGURE 7 | Temporal evolution of standardized anomaly for *in situ* and satellite Net Primary Production (NPP, **A**), temporal evolution of the Oceanic Niño Index **(B)** and cumulative satellite NPP estimations by year **(C)**, climatological NPP mean with 95% confidence interval (markers and shaded area, respectively, **D**) and mean satellite-derived NPP values during El Niño, La Niña, and Neutral conditions **(E)**. Green points in NPP time series panel indicate *in situ* measurements.

EBUS (Lachkar and Gruber, 2012); this is partially explained by the presence of continental shelves in northern Peru and central Chile (Thiel et al., 2007). Nevertheless, central Chile is characterized by its intricate geometry, with gulfs, bays, islands and peninsulas generating high time-space NPP variability. A NPP spatial pattern was observed by Testa (2017) and found by Morales et al. (2013) to coincide with Chl-a distribution.

Each upwelling system is therefore considered unique in terms of its productivity. Off central Chile, the magnitude of fertilization in the photic layer appears to be significant and quasi-permanent throughout the year, not only due to the coastal upwelling present during 66% of the year, but also as a result of nutrient influx from rivers (see below). These nutrients can sustain a large population of photosynthetic organisms and in turn present a marked impact on subsequent trophic levels (Quiñones et al., 2010). We estimated mean annual NPP at 1.1 kg C m^{-2} yr^{-1} (**Figure 7D**), similar to the value determined by Daneri et al. (2000), who estimated an annual mean of ca. 1 kg C m^{-2} yr^{-1}, but lower than estimates for Benguela and Canary EBUS (Lachkar and Gruber, 2012). Cubillos et al. (1998b) estimated the primary production required to sustain central-southern Chile coastal pelagic fisheries at 0.65 kg C m^{-2} yr^{-1}, suggesting that no productive capacity limits the regional fisheries within this zone.

Seasonal Variability in NPP

The biological annual cycle has been statistically divided into three periods (**Figure 6**; **Table 4**):

Rising Period

From September to January, optimum conditions for the phytoplankton production are observed due to the

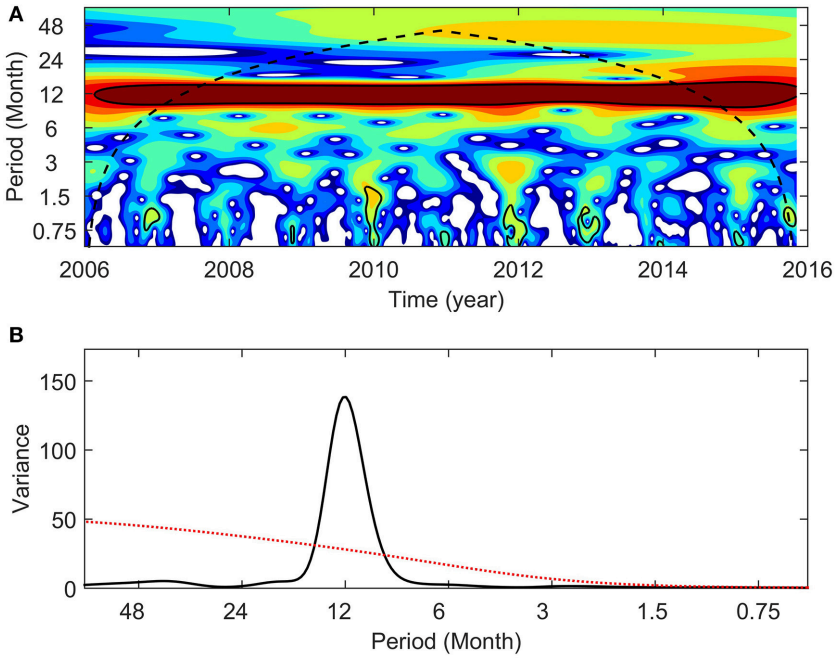

FIGURE 8 | Satellite Net Primary Production estimations wavelet power spectrum **(A)** and normalized global wavelet spectrum **(B)** with 95% confidence interval (black contours and red line, respectively). In wavelet power spectra the color scale indicates the strength of the periodicities over time (blue: weak variance; red: strong variance); the black dashed line represents the cone of influence.

synchronization of upwelling activation, optimal surface PAR values, thermal stratification and high subsurface nutrient input. During this period, NPP rates as high as 18.23 g C m^{-2} d^{-1} have been observed, with a mean integrated NPP of 4.0 g C m^{-2} d^{-1}. The strong light attenuation resulting in shallow PLD is likely to represent the main abiotic factor limiting NPP during the rising period. Nutrients, although occasionally reaching very low concentrations, were never depleted. Satellite estimations reveal a major proportion of Chl-a (and NPP) attributable to microphytoplankton (diatoms) during this period. *In situ* observations (Montero et al., 2007; Morales et al., 2007; Thiel et al., 2007; Iriarte et al., 2012; Anabalón et al., 2016) have revealed that chain-forming diatoms (*Skeletonema costatum*, *Thalassiosira* spp. and *Chaetoceros* spp.) dominate the phytoplankton community during periods of high NPP. A majority of NPP generated by diatoms is consumed by microheterotrophs (Thiel et al., 2007; Vargas et al., 2007), with only a small fraction (0–10%) of the C fixed by photosynthesis directly assimilated by copepods via the traditional herbivore food chain. Vargas et al. (2006) observed a negative relationship between egg hatching success, naupliar survival and diatom ingestion. Low direct herbivore zooplankton pressure on diatom communities may permit a proliferation of phytoplankton within this system. NPP rates of up to 18.3 (this study), 19.9 (Daneri et al., 2000) and 25.8 g C m^{-2} d^{-1} (Montero et al., 2007) have been observed, with the latter two determining the release of O_2 during photosynthesis based on changes in bulk O_2 concentration.

Falling Period

During February and March, PAR values remained adequate for supporting the phytoplankton community and the input of nutrients by coastal upwelling remained significant. Nevertheless, *in situ* NPP strongly decreased, with monthly mean values between 1.0 and 1.8 g C m^{-2} d^{-1}. Lower NPP rates and Chl-a values may result from a change in the physiological state of phytoplankton induced by biological (i.e., viral lysis; Brussaard, 2004) or physical components, such as decreases in ocean temperature and surface PAR and elevated turbulence (Garrison and Tang, 2014). The influence of top-down regulation by small ictiofauna species, particularly *Engraulis ringens*, should be considered. Cubillos et al. (1998a) observed that anchovy reached a maximum relative abundance between February and May, and stomach content analysis demonstrated that this specie is an omnivore and displays a preference for phytoplankton (Arrizaga et al., 1993).

Basal Period

In situ NPP revealed a mean basal productivity from May to August of 12% of spring-summer productivity, and a NPPE of approximately 24% of spring-summer values for the same period. Basal productivity (averaging 1.01 and 0.46 g C m^{-2} d^{-1} for NPPE and *in situ* measurements, respectively) may be supported by nutrient influx associated with continental runoff and river discharge. Maximum river discharge is correlated with precipitation in winter (Sobarzo et al., 2007). River discharge to the coastal zone produced a plume extending to the fixed station under study (Saldías et al., 2012). Northern wind patterns

observed during the study period are known to drive the downwelling of subantartic waters SAAW (Silva et al., 2009) and consequential mixing with fresh water inputs. In this way, SAAW water appears to maintain relatively lower, but continued productivity. Sobarzo et al. (2007) show that wind was too weak to disrupt the buoyancy stratification around the river mouth at any point during the year. Indeed, continental freshwater discharge increased water column stability and inhibited wind-driven vertical mixing. As a result, greater residence times in the water column were observed during winter (Montecino et al., 2006). More intense stratification, together with nutrients input from river discharge, may create favorable conditions for the growth of nano- and picophytoplankton communities (Iriarte et al., 2012).

During the wet season, higher stratification and a decrease in phytoplankton biomass (due to a reduced cell size) may create advantageous conditions for light penetration within the water column. In spite of lower surface PAR values, the 1% limit occurs at a greater depth. As a result, more homogenous Chl-a concentrations were observed within the upper 30 m during winter, with NPP resulting from the integration of a deeper layer. Comparable photosynthetic efficiency was found as compared to phytoplankton groups characterizing the upwelling season. *In situ* measurements of phytoplankton size classes (i.e., Collado-Fabbri et al., 2011; Iriarte et al., 2012; Velasco et al., in preparation) have shown that the empirical equations provided by Hirata et al. (2011) underestimate the nanophytoplankton community and overestimate microphytoplankton communities during the winter season, which can be attributed to elevated satellite Chl-a values within the area. Seasonal cycles of NO_3^-, PO_4^{3-} and $Si(OH)_4$ appear to be partially controlled by coastal upwelling, continental discharge, alterations in water masses (ESSW and SAAW) and nutrient uptake by phytoplankton groups.

Poor light attenuation near ST18 during winter suggests that particulate matter transported by the river plume may be predominantly deposited within the river terrace; therefore they do not affect the waters of the continental shelf (Saldías et al., 2012). However, inorganic nutrients from riverine sources seem to reach a greater area, as shown by high near-surface $Si(OH)_4$ concentrations observed at ST18 (located ∼27 km from the Itata River mouth). The study of seasonal continental and oceanic nutrient fluxes in this zone (**Figure 4**) reveals that during the wet season the Itata River is a primary source of $Si(OH)_4$ (11.4 times higher than the contribution of wind-driven costal upwelling). Hickey and Banas (2008) suggested that watershed-derived nutrients may help sustain productivity of the coastal ecosystem around the Columbia River during periods of weak upwelling-favorable winds and during periods of downwelling. These results indicate a smaller scale but similar dynamic within our study zone, and support an understanding of the zone off central Chile as one of the most productive in the world, even under non-upwelling conditions (Montecino et al., 2004). Hutchins et al. (2002) and Messié and Chavez (2015) identified an iron limitation on NPP in the northern zone of the Humboldt EBUS, particularly during austral winter. Itata River discharge may represent an important source of dissolved iron to our study zone (DGA, 2004; Salamanca and Pantoja, 2009), while helping to sustain high NPP near the river mouth during the non-upwelling season.

Surface salinity climatology (**Figure 3B**) differed from the results presented by Sobarzo et al. (2007), especially between September and December. We attributed this difference to surface salinity dynamics during 2014 and 2015 (e.g., surface salinity fluctuated between 20.34 and 32.96 from August to November 2014; Supplementary Figure 2). We recognized this period as anomalous, since 2014 and 2015 deviate from the observed trend of water column cooling and sea surface salinity increase at ST18, especially during the austral winter (Schneider et al., 2017). Cumulative Itata River runoff data from August to November 2014 reached decadal highs (Supplementary Figure 4). As a result, the cumulative NPPE value for November 2014 was one of the lowest of the decade (**Figure 7C**). Changes to river runoff timing may modify the division of the annual biological cycle as observed by cluster analysis. A potential variation in basal productivity magnitude and timing in river-influenced zones over the continental shelf plays a fundamental ecological role, as a greater abundance of *E. ringens* and *Strangomera bentincki* in early life stages (eggs and larvae) was observed during this season and at salinities between 32 and 34 (Soto-Mendoza et al., 2010). Additionally, increased stratification of the water column may favor a greater downward carbon flux (605 mg C m^{-2} d^{-1}) as compared to other periods of the year (between 152 and 268 mg C m^{-2} d^{-1}; Vargas et al., 2007).

NPP Hot Moments and Weekly Variability

This is the first study of NPP variability over an extended time period in this area, combining measurements and estimates to complement established understanding of coastal upwelling (Montero et al., 2007; Sobarzo et al., 2007). The continental shelf is also subjected to other kinds of variability, and one cause of misalignments between measurements and estimates of NPP are the high frequency variations in the relaxed and active phases of upwelling events, which cause variations in the microbiological community and production rates. *In situ* NPP measurements for ST18 reveal the occurrence of events where LCAR were highly increased (or "hot moments" as described by McClain et al., 2003). Peaks as high as 18.2 g C m^{-2} d^{-1} (October 2006) do not appear to be reflected by NPPE. This may be explained by the fact that NPP peaks lasted less than 8 days and/or covered an area of less than 81 km^2, and NPPE for the closest pixel to ST18 is unable to capture this level of variability; in general the hot moment's phenomenon is poorly documented. Farías et al. (2015) observed that nitrous oxide hot moments in central Chile are positively correlated with phytoplankton biomass, although these events do not specifically occur with high wind stress or with colder water. Effective Chl-a accumulation requires an optimal window of 3–7 days of reduced winds (Farías et al., 2015). It may be necessary to carry out daily, weekly and intra-seasonal investigations to identify NPP hot moments and avoid underestimations of NPP for this region during the upwelling season. Synoptic processes including active and relaxed coastal upwelling events and coastal waves may result in poor correlation between *in situ* and satellite-derived NPP during the upwelling season (**Table 3**). Monthly measurements are unable to

capture variability, and therefore generate a standard deviation that explains estimated and measured NPP rates. Week-to-week (WW) temporal variability presented in **Figure 9** varies between −5.33 and 3.15 g C m^{-2} d^{-1}, with a mean value ± SD of 0.72 ± 0.74 g C m^{-2} d^{-1} ($n = 454$). Absolute magnitude for maximum (>1.1 g C m^{-2} d^{-1}) WW monthly mean variability was observed from November to January, while lower (<0.32 g C m^{-2} d^{-1}) estimations were calculated between May and July (**Figure 9B**). Daneri et al. (2012) calculated up to a six-fold difference in WW gross primary production at a near-coast station within our study zone during the austral summer. We consider that a higher standard deviation in NPP and subsurface nutrients during spring-summer may also be caused by intense mesoscale activity (Morales et al., 2007), since a higher number of oceanic eddies were observed in the Peru-Chile current system for this period (Letelier, 2010). On the other hand, lower WW variability in NPP during the austral winter (**Figure 9**) may explain the higher coefficient of determination between *in situ* and satellite NPP (**Table 3**) for this period.

ENSO Effect on NPP Interannual Variability

Modest interannual variability was detected over the study period, with the highest NPPE variability observed during neutral years between 2006 and 2015 (**Figure 7**). The maximum cumulative PAR observed in 2014–15 (Supplementary Figure 4) may explain the highest observed NPPE values. On the other hand, minimum cumulative NPPE observed during 2012–2013 may be explained by a deficit in subsurface nutrient input (Supplementary Figure 2).

No statistical significance was found for NPPE between EN and LN conditions at 36°S. Iriarte and González (2004) suggested that the ENSO cycle affected NPP and water column properties in northern Chile (23°S) during the EN 1997–98, as compared with the non-EN period, driving a shift toward a major proportion of pico- and nanophytoplankton and decreasing NPP rates. Contrarily, Ulloa et al. (2001) and Pizarro et al. (2002) found no significant alteration in phytoplankton biomass in coastal waters close to this latitude during EN 1998. A similar ambiguity was observed at 36°S during the 2006–2015 ENSO cycles, which were less strong than previous events (i.e., EN 1997–98). *In situ* monthly surveys struggle to effectively capture the ENSO effect on bio-physicochemical properties in central Chile, while the use of remote sensing data may be a useful tool to increase the robustness of these observations. Corredor-Acosta et al. (2015) revealed that the effect of ENSO-related climate variability on Chl-a was relatively weak in the coastal zone, and this study observed no statistical significance for NPPE between EN and LN conditions, perhaps due to the distance from the equator. Nevertheless, a study over a longer time series and covering more intense EN and LN events is recommended in order to improve understanding of the ENSO effect on NPP off the coast of central Chile.

CONCLUSION

The analysis of a decade of bio-oceanographic information allowed for the identification of the main seasonal patterns modulating the annual biological cycle, which can be divided into three stages (i.e., rising, falling and basal).

The magnitude of fertilization in the photic layer appears to be significant and quasi-permanent throughout the year, not only due to the coastal upwelling present during 66% (from September to April) of the year, but also as a result of nutrient influx from rivers (from May to August). Specifically, the Itata River discharge during austral winter may partially support basal productivity around the river mouth, as a result of nutrient input and the influence of the fresh water plume on water column stratification.

Weekly and synoptic variability intensely influence the NPP annual cycle, especially during the upwelling season, which may explain the poor correlation between *in situ* and satellite-derived NPP for this season.

The ENSO cycle does not appear to impact annual NPP estimates for the study area, which was estimated at 1.1 kg C m^{-2} yr^{-1}.

This research presents relevant insights regarding NPP temporal variability in an upwelling area. The NPP baseline provided by this study may be useful in gaining improved understanding of how NPP responds to natural and human-induced changes in wind patterns and rivers runoff regimes. Changes in the NPP annual cycle, magnitude and timing may alter the carbon cycle and heterotrophic population dynamics and therefore present important implications for biogeochemical and ecological equilibriums.

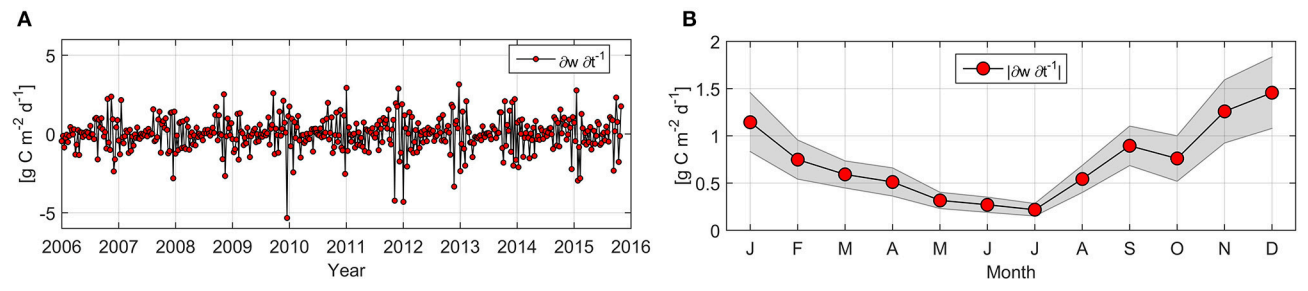

FIGURE 9 | Temporal evolution **(A)** and absolute climatology mean **(B)** for Net Primary Production week-to-week variability. Shaded area represents a 95% confidence interval.

AUTHOR CONTRIBUTIONS

LF provided in situ biogeochemical data from the fixed time series station; IM provided the VGPM estimations; GT supplied satellite data and the three authors wrote and analyzed data for the manuscript.

FUNDING

This research was funded by the Center of Excellence FONDAP-CONYCIT N° 15110009, FONDECYT N° 1161138 (LF) and GT was supported by CONICYT-PFCHA/Doctorado Nacional/2017-21170561.

ACKNOWLEDGMENTS

The authors thank the biogeochemistry group of the Universidad de Concepción for their help and support. We also thank F. Tapia, M. Sobarzo, C. Morales, R. Escribano, W. Schneider, and reviewers for their valuable comments and suggestions.

SUPPLEMENTARY MATERIAL

The Supplementary Material for this article can be found online at: https://www.frontiersin.org/articles/10.3389/fmars.2018.00179/full#supplementary-material

REFERENCES

Aguirre, C., Garreaud, R. D., and Rutllant, J. A. (2014). Surface ocean response to synoptic-scale variability in wind stress and heat fluxes off south-central Chile. *Dyn. Atmos. Oceans* 65, 64–85. doi: 10.1016/j.dynatmoce.2013.11.001

Anabalón, V., Morales, C. E., González, H. E., Menschel, E., Schneider, W., Hormazabal, S., et al. (2016). Micro-phytoplankton community structure in the coastal upwelling zone off Concepción (central Chile): annual and inter-annual fluctuations in a highly dynamic environment. *Prog. Oceanogr.* 149, 174–188. doi: 10.1016/j.pocean.2016.10.011

Arrizaga, A., Fuentealba, M., Espinoza, C., Chong, J., and Oyarzun, C. (1993). Hábitos tróficos de dos especies de peces pelágicos, la sardina *Strangomera bentincki* y la anchoveta *Engraulis ringens*, en el litoral de la Región del Bío-Bío, Chile. *Bol. Soc. Biol.* 64, 27–35.

Bakun, A. (1973). *Coastal Upwelling Indices, West Coast of North America, 1946-71*. Seattle, WA: National Oceanic and Atmospheric Administration.

Banse, K. (2002). Should we continue to measure ^{14}C-uptake by phytoplankton for another 50 years. *Limnol. Oceanogr Bull.* 11, 45–46.

Behrenfeld, M. J., Boss, E., Siegel, D. A., and Shea, D. M. (2005). Carbon-based ocean productivity and phytoplankton physiology from space. *Global Biogeochem. Cycles* 19:GB1006. doi: 10.1029/2004GB002299

Behrenfeld, M. J., and Falkowski, P. G. (1997a). A consumer's guide to phytoplankton primary productivity models. *Limnol. Oceanogr.* 42, 1479–1491.

Behrenfeld, M. J., and Falkowski, P. G. (1997b). Photosynthetic rates derived from satellite-based chlorophyll concentration. *Limnol. Oceanogr.* 42, 1–20. doi: 10.4319/lo.1997.42.1.0001

Bender, M. L., Grande, K., Johnson, K., Marra, J., Williams, P. J., Le, B., et al. (1987). A comparison of four methods for determining planktonic community production. *Limnol. Oceanogr.* 32, 1085–1098.

Boiser, J. P., Rondanelli, R., Garreaud, R. D., and Muñoz, F. (2016). Anthropogenic and natural contributions to the Southeast Pacific precipitation decline and recent megadrought in central Chile. *Geophys. Res. Lett.* 43, 413–421. doi: 10.1002/2015GL067265

Boyer, T., Conkright, M. E., and Levitus, S. (1999). Seasonal variability of dissolved oxygen, percent oxygen saturation, and apparent oxygen utilization in the Atlantic and Pacific Oceans. *Deep Sea Res. I* 46, 1593–1613. doi: 10.1016/S0967-0637(99)00021-7

Brussaard, C. P. (2004). Viral control of phytoplankton populations–a review. *J. Eukaryot. Microbiol.* 51, 125–138. doi: 10.1111/j.1550-7408.2004.tb00537.x

Cai, W. J., Dai, M., and Wang, Y. (2006). Air-sea exchange of carbon dioxide in ocean margins: a province-based synthesis. *Geophys. Res. Lett.* 33:L12603 doi: 10.1029/2006GL026219

Collado-Fabbri, S., Vaulot, D., and Ulloa, O. (2011). Structure and seasonal dynamics of the eukaryotic picophytoplankton community in a wind-driven coastal upwelling ecosystem. *Limnol. Oceanogr.* 56, 2334–2346. doi: 10.4319/lo.2011.56.6.2334

Corredor-Acosta, A., Morales, C. E., Hormazábal, S., Andrade, I., and Correa-Ramirez, M. A. (2015). Phytoplankton phenology in the coastal upwelling region off central-southern Chile (35°S–38°S): time-space variability, coupling to environmental factors, and sources of uncertainty in the estimates. *J. Geophys. Res. Ocean.* 120, 813–831. doi: 10.1002/2014JC010330

Cubillos, S. L., Canales, M., Hernández, R. A., Bucarey, S. D., Vilugrón, L., and Miranda, A. L. (1998b). Poder de pesca, esfuerzo de pesca y cambios estacionales e interanuales en la abundancia relativa de *Strangomera bentincki* y *Engraulis ringens* en el área frente a Talcahuano, Chile (1990-97). *Rev. Invest. Mar.* 26, 3–14.

Cubillos, S. L., Nuñez, S., and Arcos, D. (1998a). Producción primaria requerida para sustentar el desembarque de peces pelágicos en Chile. *Rev. Invest. Mar.* 26, 83–108. doi: 10.4067/S0717-71781998002600008

Cullen, J. J. (2001). "Primary production methods," in *Encyclopedia of Ocean Sciences*, ed J. H. Steele (Oxford: Academic Press), 578–584.

DGA (2004). *Diagnóstico y Clasificación de los Cursos y Cuerpos de Agua Según Objetivos de Calidad*. Cuenca del Rio Itata. Dirección General de Aguas.

Daneri, G., Dellarossa, V., Quiñones, R., Jacob, B., Montero, P., and Ulloa, O. (2000). Primary production and community respiration in the Humboldt Current System off Chile and associated oceanic areas. *Mar. Ecol. Prog. Ser.* 197, 41–49. doi: 10.3354/meps197041

Daneri, G., Lizárraga, L., Montero, P., González, H. E., and Tapia, F. J. (2012). Wind forcing and short-term variability of phytoplankton and heterotrophic bacterioplankton in the coastal zone of the Concepción upwelling system (Central Chile). *Prog. Oceanogr.* 92–95, 92–96. doi: 10.1016/j.pocean.2011.07.013

Escribano, R., Daneri, G., Farías, L., Gallardo, V. A., González, H. E., Gutiérrez, D., et al. (2004). Biological and chemical consequences of the 1997–1998 El Niño in the Chilean coastal upwelling system: a synthesis. *Deep Sea Res. II* 51, 2389–2411. doi: 10.1016/j.dsr2.2004.08.011

Escribano, R., and Schneider, W. (2007). The structure and functioning of the coastal upwelling system off central/southern Chile. *Prog. Oceanogr.* 75, 343–347. doi: 10.1016/j.pocean.2007.08.020

FAO (2014). *The State of World Fisheries and Aquaculture*. Opportunities and challenges. Rome: Food and Agriculture Organization of the United Nations.

Farías, L., Besoain, V., and García-Loyola, S. (2015). Presence of nitrous oxide hotspots in the coastal upwelling area off central Chile: an analysis of temporal variability based on ten years of a biogeochemical time series. *Environ. Res. Lett.* 10:44017. doi: 10.1088/1748-9326/10/4/044017

Farías, L., Chuecas, L. A., and Salamanca, M. A. (1996). Effect of coastal upwelling on nitrogen regeneration from sediments and ammonium supply to the water column in Concepción Bay, Chile. *Estuar. Coast. Shelf Sci.* 43, 137–155. doi: 10.1006/ecss.1996.0062

Farías, L., Fernández, C., Faúndez, J., Cornejo, M., and Alcaman, M. E. (2009). Chemolithoautotrophic production mediating the cycling of the greenhouse gases N2O and CH4 in an upwelling ecosystem. *Biogeosciences* 6, 3053–3069. doi: 10.5194/bg-6-3053-2009

Fennel, K. (2010). The role of continental shelves in nitrogen and carbon cycling: Northwestern North Atlantic case study. *Ocean Sci. J.* 6, 539–548. doi: 10.5194/os-6-539-2010

Fernández, C., Raimbault, P., Garcia, N., and Rimmelin, P. (2005). An estimation of annual new production and carbon fluxes in the northeast Atlantic Ocean during 2001. *J. Geophys. Res.* 110:C07S13. doi: 10.1029/2004JC002616

Fuenzalida, R., Schneider, W., Garcés-Vargas, J., and Bravo, L. (2008). Satellite altimetry data reveal jet-like dynamics of the humboldt current. *J. Geophys. Res.* 113:C07043. doi: 10.1029/2007JC004684

Garrison, H. S., and Tang, K. W. (2014). Effects of episodic turbulence on diatom mortality and physiology, with a protocol for the use of Evans Blue stain for live–dead determinations. *Hydrobiologia* 738, 155–170. doi: 10.1007/s10750-014-1927-0

Graco, M., Gutiérrez, D., and Farías, L. (2006). Inter-annual variability of the pelagic-benthic coupling in the upwelling system off central Chile. *Adv. Geosci.* 6, 127–132. doi: 10.5194/adgeo-6-127-2006

Grasshoff, K., Ehrhardt, M., and Kremling, K. (1983). *Methods of Seawater Analysis*. Basel: Springer-Verlag.

Henríquez, L. A., Daneri, G., Muñoz, C. A., Montero, P., Veas, R., and Palma, A. T. (2007). Primary production and phytoplanktonic biomass in shallow marine environments of central Chile: effect of coastal geomorphology. *Estuar. Coast. Shelf Sci.* 73, 137–147. doi: 10.1016/j.ecss.2006.12.013

Hickey, B. M., and Banas, N. S. (2008). Why is the northern end of the California current system so productive? *Oceanography* 21, 90–107. doi: 10.5670/oceanog.2008.07

Hirata, T., Hardman-Mountford, N. J., Barlow, R., Lamont, T., Brewin, R. J. W., Smyth, T., et al. (2009). An inherent optical property approach to the estimation of size-specific photosynthetic rates in eastern boundary upwelling zones from satellite ocean colour: an initial assessment. *Prog. Oceanogr.* 83, 393–397. doi: 10.1016/j.pocean.2009.07.019

Hirata, T., Hardman-Mountford, N. J., Brewin, R. J. W., Aiken, J., Barlow, R., Suzuki, K., et al. (2011). Synoptic relationships between surface Chlorophyll-a and diagnostic pigments specific to phytoplankton functional types. *Biogeosciences* 8, 311–327. doi: 10.5194/bg-8-311-2011

Hutchins, D. A., Hare, C. E., Weaver, R. S., Zhang, Y., Firme, G. F., DiTullio, G. R., et al. (2002). Phytoplankton iron limitation in the Humboldt Current and Peru upwelling. *Limnol. Oceanogr.* 47, 997–1011. doi: 10.4319/lo.2002.47.4.0997

Iriarte, J. L., and González, H. E. (2004). Phytoplankton size structure during and after the 1997/98 El Niño in a coastal upwelling area of the northern Humboldt current system. *Mar. Ecol. Prog. Ser.* 269, 83–90. doi: 10.3354/meps269083

Iriarte, J. L., Vargas, C. A., Tapia, F. J., Bermúdez, R., and Urrutia, R. E. (2012). Primary production and plankton carbon biomass in a river-influenced upwelling area off Concepción, Chile. *Prog. Oceanogr.* 92–95, 97–109. doi: 10.1016/j.pocean.2011.07.009

Kahru, M., Kudela, R., Manzano-Sarabia, M., and Mitchell, B. G. (2009). Trends in primary production in the California current detected with satellite data. *J. Geophy. Res.* 114:C02004. doi: 10.1029/2008JC004979

Kämpf, J., and Chapman, P. (2016). *Upwelling Systems of the World. A Scientific Journey to the Most Productive Marine Ecosystems.* Cham: Springer International Publishing.

Kirk, J. T. O. (1983). *Light & Photosynthesis in Aquatic Ecosystem*. New York, NY: Cambridge University Press.

Lachkar, Z., and Gruber, N. (2012). A comparative study of biological production in eastern boundary upwelling systems using an artificial neural network. *Biogeosciences* 9, 293–308. doi: 10.5194/bg-9-293-2012

Legendre, P., and Legendre, L. (1998). *Numerical Ecology*. Amsterdam: Elsevier Science.

Letelier, J. (2010). *Surgencia y estructuras de mesoescala frente a Chile (18°-42°S).* [Ph.D. thesis]. [Concepción]: Universidad de Concepción

Letelier, J., Pizarro, O., and Nuñez, S. (2009). Seasonal variability of coastal upwelling and the upwelling front off central Chile. *J. Geophys. Res.* 114:C12009. doi: 10.1029/2008JC005171

McClain, M. E., Boyer, E. W., Dent, C. L., Gergel, S. E., Grimm, N. B., Groffman, P. M., et al. (2003). Biogeochemical hot spots and hot moments at the interface of terrestrial and aquatic ecosystems. *Ecosystems* 6, 301–312. doi: 10.1007/s10021-003-0161-9

Messié, M., and Chavez, F. P. (2015). Seasonal regulation of primary production in estern boundary upwelling systems. *Prog. Oceanog.* 134, 1–18. doi: 10.1016/j.pocean.2014.10.011

Montecino, V., Astoreca, R., Alarcón, G., Retamal, L., and Pizarro, G. (2004). Bio-optical characteristics and primary productivity during upwelling and non-upwelling conditions in a highly productive coastal ecosystem off central Chile (∼36°S). *Deep Sea Res. II* 51, 2413–2426. doi: 10.1016/j.dsr2.2004.08.012

Montecino, V., Pizarro, G., and Quiroz, D. (1998). "Primary production in the Chilean coast," in *Biotic Impact of Extratropical Climate Variability in the Pacific*, eds G. Holloway and D. Henderson (Honolulu, HI: SOEST), 69–76.

Montecino, V., Strub, T., Chavez, F., Thomas, A., Tarazona, J., and Baumgartner, T. (2006). Chapter 10 "Bio-physical interactions off Western South-America," in *The Sea. The Global Coastal Ocean: Interdisciplinary Regional Studies and Synthesis,* Vol. 14A, eds A. R. Robinson and K. H. Brink (Cambridge: Harvard Press).

Montecinos, A., and Aceituno, P. (2003). Seasonality of the ENSO-related rainfall variability in Central Chile and associated circulation anomalies. *J. Clim.* 16, 281–296. doi: 10.1175/1520-0442(2003)016<0281:SOTERR>2.0.CO;2

Montecinos, A., and Gomez, F. (2010). ENSO modulation of the upwelling season off southern-central Chile. *Geophys. Res. Lett.* 37:L02708. doi: 10.1029/2009GL041739

Montero, P., Daneri, G., Cuevas, A. L., González, H. E., Jacob, B., Lizárraga, L., et al. (2007). Productivity cycles in the coastal upwelling area off Concepcion: the importance of diatoms and bacterioplankton in the organic carbon flux. *Prog. Oceanogr.* 75, 518–530. doi: 10.1016/j.pocean.2007.08.013

Morales, C. E., González, H. E., Hormazábal, S. E., Yuras, G., Letelier, J., and Castro, L. R. (2007). The distribution of chlorophyll-a and dominant planktonic components in the coastal transition zone off Concepción, central Chile, during different oceanographic conditions. *Prog. Oceanogr.* 75, 452–469. doi: 10.1016/j.pocean.2007.08.026

Morales, C. E., Hormazabal, S., Andrade, I., and Correa-Ramirez, M. A. (2013). Time-space variability of Chlorophyll-a and associated physical variables within the region off central-southern Chile. *Remote Sens.* 5, 5550–5571. doi: 10.3390/rs5115550

Swirgon, M., and Stramska, M. (2015). Comparison of *in situ* and satellite ocean color determinations of particulate organic carbon concentration in the global ocean. *Oceanologia* 57, 25–31. doi: 10.1016/j.oceano.2014.09.002

Neira, S., and Arancibia, H. (2004). Trophic interactions and community structure in the upwelling system off Central Chile (33–39°S). *J. Exp. Mar. Biol. Ecol.* 312, 349–366. doi: 10.1016/j.jembe.2004.07.011

Nevison, C. D., Lueker, T. J., and Weiss, R. F. (2004). Quantifying the nitrous oxide source from coastal upwelling *Global Biogeochem. Cycles* 18:GB1018. doi: 10.1029/2003GB002110

Parsons, T., Maita, Y., and Lalli, C. (1984). *A Manual of Chemical and Biological Methods for Seawater Analysis*. Oxford: Pergamon Press.

Pauly, D., and Christensen, V. (1995). Primary production required to sustain global fisheries. *Nature* 374, 255–257. doi: 10.1038/374255a0

Pizarro, G., Iriarte, J., and Montecino, V. (2002). Mesoscale primary production and bio-optical variability off Antofagasta (23-24° S) during the transition to El Niño 1997–1998. *Rev. Chil. Hist. Nat.* 75, 201–215. doi: 10.4067/S0716-078X2002000100019

Pizarro, O. (1999). *Low Frequency fluctuations in the Eastern Boundary Current off South America: Remote and Local Forcing*. Ph.D. thesis, University of Göteborg, Göteborg.

Quiñones, R. A., Gutiérrez, M. H., Daneri, G., Gutierrez, D., González, H. E., and Chavez, F. (2010). "The humboldt current system," in *Carbon and Nutrient Fluxes in Continental Margins. A Global Synthesis*, eds K. K. Liu, L. Atkinson, R. Quiñones, and L. Talaue-McManus (Berlin: Springer), 44–64.

Raimbault, P., Diaz, F., Pouvesle, W., and Boudjellal, B. (1999). Simultaneous determinations of particulate organic carbon, nitrogen and phosphorus collected on filters, using a semiautomatic wet-oxidation method. *Mar. Ecol. Prog. Ser.* 180, 289–295. doi: 10.3354/meps180289

Regaudie-de-Gioux, A., Lasternas, S., Agustí, S., and Duarte, C. M. (2014). Comparing marine primary production estimates through different methods and development of conversion equations. *Front. Mar. Sci.* 1:19. doi: 10.3389/fmars.2014.00019

Ryther, J. H., and Dunstan, W. M. (1971). Nitrogen, phosphorus, and eutrophication in the coastal marine environment. *Science* 171, 1008–1013. doi: 10.1126/science.171.3975.1008

Salamanca, M. A., and Pantoja, S. (2009). "Caracterización química de la zona marina adyacente a la desembocadura del río Itata," in *La Cuenca Hidrográfica del río Itata. Aportes Científicos Para su Gestión Sustentable*, eds O. Parra, J. C. Castilla, H. Romero, R. Quiñones, and A. Comaño (Concepción: Editorial Universidad de Concepción), 177–191.

Saldías, G. S., Sobarzo, M., Largier, J., Moffat, C., and Letelier, R. M. (2012). Seasonal variability of turbid river plumes off central Chile base on high-resolution MODIS imagery. *Remote Sens. Environ.* 123, 220–233. doi: 10.1016/j.rse.2012.03.010

Sánchez, G. E., Pantoja, S., Lange, C. B., González, H. E., and Daneri, G. (2008). Seasonal changes in particulate biogenic and lithogenic silica in the upwelling system off Concepción (∼36°S), Chile, and their relationship to fluctuations in marine productivity and continental input. *Cont. Shelf Res.* 28, 2594–2600. doi: 10.1016/j.csr.2008.07.010

Schneider, W., Donoso, D., Garcés-Vargas, J., and Escribano, R. (2017). Water-column cooling and sea surface salinity increase in the upwelling region off central-south Chile driven by a poleward displacement of the South Pacific High. *Prog. Oceanogr.* 151, 38–48. doi: 10.1016/j.pocean.2016.11.004

Silva, N., Rojas, N., and Fedele, A. (2009). Water masses in the Humboldt Current System: properties, distribution, and the nitrate deficit as a chemical water mass tracer for Equatorial Subsurface Water off Chile. *Deep Sea Res. II* 56, 1004–1020. doi: 10.1016/j.dsr2.2008.12.013

Slawyk, G., Collos, Y., and Auclair, J. C. (1977). The use of the 13C and 15N isotopes for the simultaneous measurements of carbon and nitrogen turnover rates in marine phytoplankton. *Limnol. Oceanogr.* 22, 925–932. doi: 10.4319/lo.1977.22.5.0925

Sobarzo, M., Bravo, L., Donoso, D., Garcés-Vargas, J., and Schneider, W. (2007). Coastal upwelling and seasonal cycles that influence the water column over the continental shelf off central Chile. *Prog. Oceanogr.* 75, 363–382. doi: 10.1016/j.pocean.2007.08.022

Sobarzo, M., and Djurfeldt, L. (2004). Coastal upwelling process on a continental shelf limited by submarine canyons, Concepción, central Chile. *J. Geophys. Res.* 109:C12012. doi: 10.1029/2004JC002350

Sobarzo, M., Saldías, G. S., Tapia, F. J., Bravo, L., Moffat, C., and Largier, J. L. (2016). On subsurface cooling associated with the Biobío River Canyon (Chile). *J. Geophys. Res Ocean.* 121, 4568–4584. doi: 10.1002/2016JC011796

Soto-Mendoza, S., Castro, L. R., and Llanos-Rivera, A. (2010). Variabilidad espacial y temporal de huevos y larvas de *Strangomera bentincki* y *Engraulis ringens*, asociados a la desembocadura del río Itata, Chile. *Rev. Biol. Mar. Oceanogr.* 45, 471–487. doi: 10.4067/S0718-19572010000300012

Steeman Nielsen, E. (1952). The use of radioactive carbon (^{14}C) for measuring production in the sea. *J. Cons. Perm. Int. Explor. Mer.* 18, 117–140.

Sydeman, W. J., García-Reyes, M., Schoeman, D. S., Rykaczewski, R. R., Thompson, S. A., Black, B. A., et al. (2014). Climate change and wind intensification in coastal upwelling ecosystems. *Science* 345, 77–80. doi: 10.1126/science.1251635

Testa, G. (2017). *Variabilidad Espacio-Temporal de la Productividad Primaria Neta en la Plataforma Continental de Chile Central (73°W-36°S); Causas y Consecuencias*. Master's Thesis, Universidad de Concepción, Concepción.

Thiel, M., Macaya, E. C., Acuña, E., Arntz, W. E., Bastias, H., Brokordt, K., et al. (2007). The humboldt current system of Northern and Central Chile. *Oceanogr. Mar. Biol. Annu. Rev.* 45, 195–344. doi: 10.1201/9781420050943.ch6

Torrence, C., and Compo, G. P. (1998). A practical guide to wavelet analysis. *Bull. Am. Meteorol. Soc.* 79, 61–78. doi: 10.1175/1520-0477(1998)079<0061:APGTWA>2.0.CO;2

Ulloa, O., Escribano, R., Hormazábal, S., Quiñones, R. A., González, R. R., and Ramos, M. (2001). Evolution and biological effect of the 1997-98 El Niño in the upwelling ecosystem off northern Chile. *Geophys. Res. Lett.* 28, 1591–1594. doi: 10.1029/2000GL011548

Vargas, C. A., Escribano, R., and Poulet, S. (2006). Phytoplankton food quality determines time windows for successful zooplankton reproductive pulses. *Ecol.* 87, 2992–2999. doi: 10.1890/0012-9658(2006)87[2992:PFQDTW]2.0.CO;2

Vargas, C. A., Martínez, R. A., Cuevas, L. A., Pavez, M. A., Cartes, C., González, H. E., et al. (2007). The relative importance of microbial and classical food webs in a highly productive coastal upwelling area. *Limnol. Oceanogr.* 52, 1495–1510. doi: 10.4319/lo.2007.52.4.1495

Conflict of Interest Statement: The authors declare that the research was conducted in the absence of any commercial or financial relationships that could be construed as a potential conflict of interest.